Dalton Transactions

PAPER

View Article Online
View Journal | View Issue

Cite this: *Dalton Trans.*, 2016, **45**, 361

Halide coordinated homoleptic $[Fe_4S_4X_4]^{2-}$ and heteroleptic $[Fe_4S_4X_2Y_2]^{2-}$ clusters (X, Y = Cl, Br, I)—alternative preparations, structural analogies and spectroscopic properties in solution and solid state†

Andreas O. Schüren,[a,b] Verena K. Gramm,[a] Maximilian Dürr,[c] Ana Foi,[b] Ivana Ivanović-Burmazović,[c] Fabio Doctorovich,[b] Uwe Ruschewitz[a] and Axel Klein*[a]

Received 21st July 2015,
Accepted 10th November 2015

DOI: 10.1039/c5dt02769a

www.rsc.org/dalton

New facile methods to prepare iron sulphur halide clusters $[Fe_4S_4X_4]^{2-}$ from $[Fe(CO)_5]$ and elemental sulphur were elaborated. Reactions of ferrous precursors like tetrahalidoferrates(II) or simple ferrous halides with $[Fe(CO)_5]$ and sulphur turned out to be efficient methods to prepare homoleptic $[Fe_4S_4X_4]^{2-}$ (X = Cl, Br) and heteroleptic clusters $[Fe_4S_4X_{4-n}Y_n]^{2-}$ (X = Cl, Br; Y = Br, I). Solid materials were obtained as salts of $BTMA^+$ (= benzyltrimethylammonium); the new compounds containing $[Fe_4S_4Br_4]^{2-}$ and $[Fe_4S_4X_2Y_2]^{2-}$ (X, Y = Cl, Br, I) were all isostructural to $(BTMA)_2[Fe_4S_4I_4]$ (monoclinic, *Cc*) as inferred from synchrotron X-ray powder diffraction. While the solid materials contain defined heteroleptic clusters with a halide X : Y ratio of 2 : 2, dissolving these compounds leads to rapid scrambling of the halide ligands forming mixtures of all five possible $[Fe_4S_4X_{4-n}Y_n]^{2-}$ clusters as could be shown by UHR-ESI MS. The variation of X and Y allowed assignment of the absorption bands in the visible and NIR; the long-wavelength bands around 1100 nm were tentatively assigned to intervalence charge transfer (IVCT) transitions.

Introduction

Cubane-shaped $[Fe_4S_4]$ clusters represent a very interesting class of cofactors in biology and are involved in various functions in a cell's life cycle.[1–6] Due to their mixed valent character with two ferric (Fe^{III}) and two ferrous (Fe^{II}) iron atoms these clusters show extraordinary electrochemical properties which are crucial for their biological functions in electron transfer and redox catalysis reactions.[7] During the last 40 years numerous $[Fe_4S_4]^{2+}$ clusters with terminal thiolate ligands have been prepared in order to model the structural, electronic and electrochemical properties as well as the reactivity of the naturally occurring clusters.[8–16] Furthermore, several studies have recently been conducted to elucidate their availability as precursors for iron sulphur material synthesis as well as single molecule applications.[17–24] Halide based $[Fe_4S_4X_4]^{2-}$ with X = Cl, Br or I are known to be useful precursors because the halides can be easily exchanged with thiolate or other ligands by salt metathesis reactions. Homoleptic halide clusters have thus been studied previously and some preparation methods have been published (Scheme 1).[25]

They can be either formed by ligand exchange from hydrogen sulfide or thiolate coordinated $[Fe_4S_4]^{2+}$ clusters (see Scheme 1A and B) or directly starting from relatively cheap bulk chemicals.[26–28] Müller and co-workers have been able to prepare $[Fe_4S_4Cl_4]^{2-}$ and $[Fe_4S_4Br_4]^{2-}$ clusters from ferric or ferrous iron halides and excess H_2S in the presence of triethylamine as base (Scheme 1C).[29] The chloride cluster can be also synthesised from iron(II) chloride and sulphur that has been reduced *in situ* with thiophenolate (Scheme 1D).[20] A convenient preparation method for the iodide cluster using iron pentacarbonyl, sulphur, iodine and an iodide salt has been reported by Pohl and co-workers (Scheme 1E).[30,31]

[a]*Department für Chemie, Institut für Anorganische Chemie, Universität zu Köln, Greinstraße 6, 50939 Köln, Germany. E-mail: axel.klein@uni-koeln.de*
[b]*Departamento de Química Inorgánica, Analítica, y Química Física, Facultad de Ciencias Exactas y Naturales, INQUIMAE-CONICET, Universidad de Buenos Aires, Ciudad Universitaria, Pabellón 2, Piso 3, C1428EHA Buenos Aires, Argentina*
[c]*Department Chemie und Pharmazie, Lehrstuhl für Bioanorgansiche Chemie, Friedrich-Alexander-Universität Erlangen-Nürnberg, Egerlandstraße 1, 91058 Erlangen, Germany*

† Electronic supplementary information (ESI) available: Negative mode ESI mass and UV-vis-NIR spectra as well as synchrotron XRPD as mentioned in the text. See DOI: 10.1039/c5dt02769a

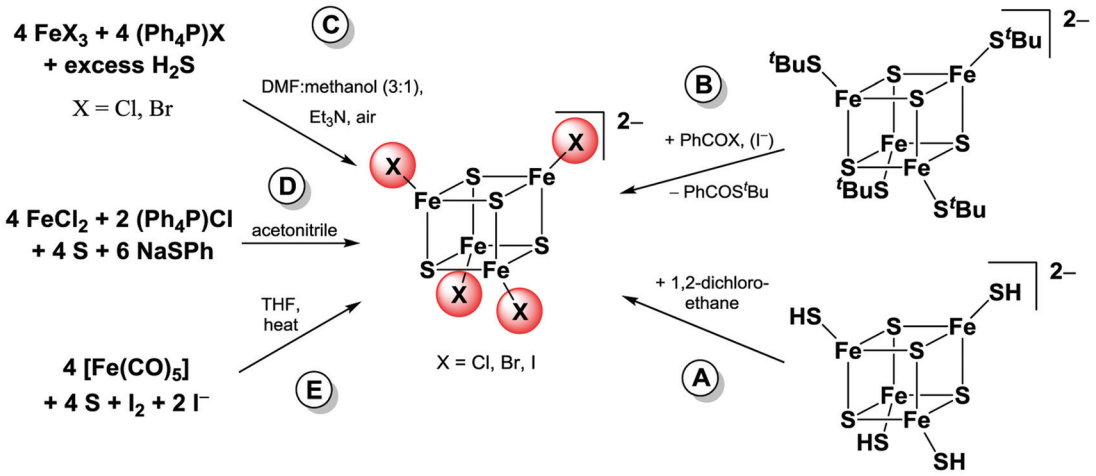

Scheme 1 Reported preparation pathways for $[Fe_4S_4X_4]^{2-}$ clusters. (Method A: Henderson *et al.*;[28] Method B: Holm *et al.*;[26,27] Method C: Müller *et al.*;[29] Method D: Kanatzidis *et al.*;[20] Method E: Pohl *et al.*[30,31]).

While many examples for $[Fe_4S_4]$ clusters with a homoleptic coordination sphere of thiolate, halide, nitrogen or phosphorus ligands are known, the number of clusters with a heteroleptic ligand set is much smaller. Although several clusters $[Fe_4S_4L_2L'_2]^{2-}$ and $[Fe_4S_4L_3L']^{2-}$ have been published exhibiting a 2 : 2 or 3 : 1 coordination sphere of two different ligand types L and L′ (L, L′ = Cl^-, Br^-, I^-, phenolates, thiophenolates and dithiocarbamates) they are very difficult to isolate. In solution the ligands are exchanged among the clusters leading to coordinative disproportionation (eqn (1)).[9,10,32,33]

$$(4-n)\,[Fe_4S_4L_4]^{2-} + n\,[Fe_4S_4L'_4]^{2-} \rightleftharpoons 4\,[Fe_4S_4L_{4-n}L'_n]^{2-} \quad (1)$$

This exchange equilibrium is hampered if the cluster's charge is neutral due to one neutral ligand type L″ like in $[Fe_4S_4I_2(Ph_3PS)_2]^{34}$ $[Fe_4S_4(SPh)_2(^tBu_3P)_2]^{35}$ or $[Fe_4S_4(SR)_2(SC(NMe_2))_2]^{36}$ (R = 2,4,6-triisopropylphenyl). The products of ligand exchange on neutral $[Fe_4S_4L_2L''_2]$ are ionic and are less favourable in non-polar solvents.[37,38] In order to completely avoid this exchange, tripodal thiolate ligands were established to stabilise clusters with 3 : 1 coordination.[39–48]

$[Fe_4S_4Br_2Cl_2]^{2-}$ is so far the only reported example of a heteroleptic halide $[Fe_4S_4]$ cluster that has been isolated and characterised in solid state.[29] The preparation of further clusters $[Fe_4S_4X_2Y_2]^{2-}$ and $[Fe_4S_4X_3Y]^{2-}$ having a 2 : 2 or 3 : 1 coordination (Scheme 2) of two different halide ligands is desirable hence these clusters will be excellent precursors for selective ligand exchange reactions to form heteroleptic clusters with more intricate ligands. Furthermore, these clusters may provide deeper insight into the electronic structure of the $[Fe_4S_4]$ core due to the different electronegativity of the halide ligands and the relatively small number of atoms.

In this contribution we will report on new, remarkably improved preparation methods for homoleptic $[Fe_4S_4X_4]^{2-}$ and heteroleptic $[Fe_4S_4X_2Y_2]^{2-}$ clusters (X = Cl, Br; Y = Br, I) modifying the above mentioned method by Pohl that was previously only reported for the preparation of the iodide cluster.[30,31] The application of iron(II) halides and related precursors turned out to be the most efficient procedure to prepare those clusters in excellent yields. By this procedure we prepared *e.g.* the new clusters $[Fe_4S_4Cl_2I_2]^{2-}$ and $[Fe_4S_4Br_2I_2]^{2-}$. Furthermore, we utilised different elemental halogens and interhalogens as well as halides to examine the scope of this procedure. The resulting materials, which were mainly salts of the $BTMA^+$ (= benzyltrimethylammonium) cation were characterised in the solid by X-ray powder diffraction (XRPD) and IR spectroscopy and in solution by ESI MS and UV-vis-NIR absorption spectroscopy.

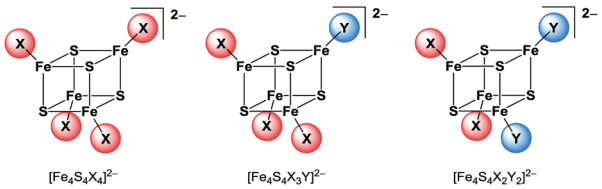

Scheme 2 Homoleptic and heteroleptic halide $[Fe_4S_4]$ cluster with 3 : 1 and 2 : 2 coordination.

Results and discussion

Preparations and analytics

It turned out that homoleptic $[Fe_4S_4X_4]^{2-}$ as well as heteroleptic $[Fe_4S_4X_2Y_2]^{2-}$ clusters can be obtained most efficiently if Pohl's method is modified by replacing one equivalent of $[Fe(CO)_5]$ and the halogen compound by simple iron(II) halide precursors (Scheme 3).

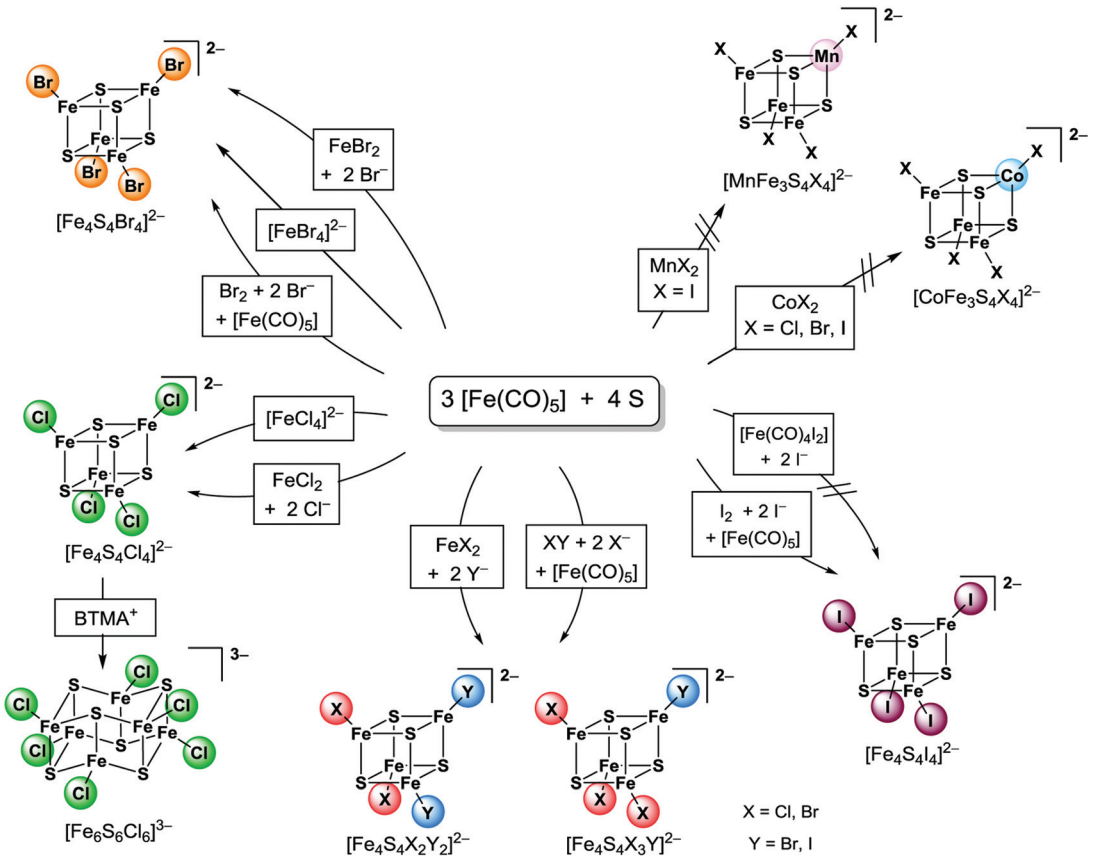

Scheme 3 Cluster preparations starting from $[Fe(CO)_5]$ and sulphur used in the present work.

Heating $[Fe(CO)_5]$, sulphur, anhydrous ferrous halides and BTMA halides ($BTMA^+$ = benzyltrimethylammonium) in MeCN for several days under an inert atmosphere allowed to obtain black, air and moisture sensitive solutions of $[Fe_4S_4Cl_4]^{2-}$ and $[Fe_4S_4Br_4]^{2-}$ (Scheme 3, eqn (2)) as confirmed by UV-vis-NIR absorption spectra (see later). The observed absorptions bands are in line with those reported for the cluster ions $[Fe_4S_4Cl_4]^{2-}$ and $[Fe_4S_4Br_4]^{2-}$.[25]

High yields (87%) of black crystalline material were obtained by slow diffusion of diethyl ether into these solutions at −18 °C. The material obtained for X = Br is $(BTMA)_2[Fe_4S_4Br_4]$. In contrast to this, the crystalline material from $[Fe_4S_4Cl_4]^{2-}$ solution was identified as the prismane shaped hexanuclear cluster $(BTMA)_3[Fe_6S_6Cl_6]$ (eqn (2), Scheme 3) although in solution the tetranuclear, cubane species $[Fe_4S_4Cl_4]^{2-}$ is stable and has been isolated previously from such solutions as salts of organic ammonium and phosphonium cations.[20–31] We assume that the tetranuclear species is dominating a mixture of several possible cluster species (bi-, tetra-, hexanuclear) which are interconnected through rearrangements.[49] The reason why crystallisation using the $BTMA^+$ ions lead to the hexanuclear species probably lies in the better crystallisation of the latter over the tetranuclear species. To verify this assumption we will try to get single crystals of corresponding compounds in the future.

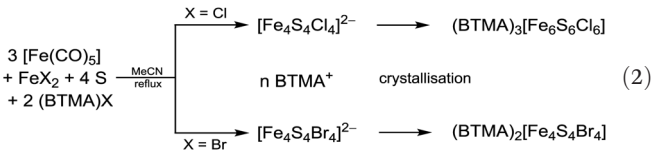

(2)

We also utilised $[FeCl_4]^{2-}$ and $[FeBr_4]^{2-}$ for cluster formation. These precursors combine the iron(II) halide and the halide source. From reactions of $(Et_4N)_2[FeCl_4]$ or $(Ph_4P)_2[FeBr_4]$, respectively, with $[Fe(CO)_5]$ and sulphur in MeCN $(Et_4N)_2[Fe_4S_4Cl_4]$ and $(Ph_4P)_2[Fe_4S_4Br_4]$ were obtained as black solids in moderate to good yields of 69–92% (Scheme 3, eqn (3), Table 1). Obviously, both cluster formation methods have the same pathway since it is known that ferrous halides form tetrahalidoferrates(II) $[FeX_4]^{2-}$ in presence of excess halide.[50] Therefore, these $[FeX_4]^{2-}$ are assumed to be intermediates for cluster assembly.

Remarkably, no product formation was observed when using ferrous iodide precursors. For example, from our attempts to perform analogous reactions with $[Fe(CO)_4I_2]$ no defined products were obtained (eqn (3)). Like with iron(II) chloride and bromide we assume a rapid formation of tetraiodidoferrate(II) in those solutions. In contrast to $[FeCl_4]^{2-}$ and $[FeBr_4]^{2-}$, $[FeI_4]^{2-}$ seems to be inert towards the desired cluster formation reactions. This is supported by the fact that crystal-

Table 1 Overview on methods for halide $[Fe_4S_4]$ cluster preparation

Compound	Starting materials	Conditions	Yield	Reference
$(BTMA)_2[Fe_4S_4I_4]$	$[Fe(CO)_5] + S_8 + I_2 + (BTMA)I$	THF, reflux	95%	30, 31
$(BTMA)_2[Fe_4S_4I_4]$	$[Fe(CO)_5] + S_8 + I_2 + (BTMA)I$	MeCN, reflux	81%	This work
$(BTMA)_2[Fe_4S_4Br_4]$	$[Fe(CO)_5] + S_8 + FeBr_2 + (BTMA)Br$	MeCN, reflux	87%	This work
$(BTMA)_2[Fe_4S_4Br_2Cl_2]$	$[Fe(CO)_5] + S_8 + FeCl_2 + (BTMA)Br$	MeCN, reflux	89%	This work
$(BTMA)_2[Fe_4S_4Cl_2I_2]$	$[Fe(CO)_5] + S_8 + FeCl_2 + (BTMA)I$	MeCN, reflux	77%	This work
$(BTMA)_2[Fe_4S_4Br_2I_2]$	$[Fe(CO)_5] + S_8 + FeBr_2 + (BTMA)I$	MeCN, reflux	85%	This work
$(Et_4N)_2[Fe_4S_4Cl_4]$	$[Fe(CO)_5] + S_8 + (Et_4N)_2[FeCl_4]$	MeCN, reflux	69%	This work
$(Ph_4P)_2[Fe_4S_4Br_4]$	$[Fe(CO)_5] + S_8 + (Ph_4P)_2[FeBr_4]$	MeCN, reflux	92%	This work
$(Ph_4P)_2[Fe_4S_4Br_4]$	$[Fe(CO)_5] + S_8 + Br_2 + (BTMA)Br$	THF, reflux	71%	This work
$(BTMA)_2[Fe_4S_4Cl_2I_2]$	$[Fe(CO)_5] + S_8 + I_2 + (BTMA)Cl$	THF, reflux	75%	This work
$(BTMA)_2[Fe_4S_4ClI_3]$	$[Fe(CO)_5] + S_8 + ICl + (BTMA)I$	THF, reflux	94%	This work
$(BTMA)_2[Fe_4S_4BrI_3]$	$[Fe(CO)_5] + S_8 + IBr + (BTMA)I$	THF, reflux	81%	This work
$(Ph_4P)_2[Fe_4S_4Cl_4]$	$FeCl_3 + (Ph_4P)Cl + H_2S$ excess	DMF, MeOH, Et_3N	80%	29
$(Ph_4P)_2[Fe_4S_4Br_4]$	$FeBr_3 + (Ph_4P)Br + H_2S$ excess	DMF, MeOH, Et_3N	78%	29
$(Ph_4P)_2[Fe_4S_4Br_2Cl_2]$	$FeBr_3 + (Ph_4P)Cl + H_2S$ excess	DMF, MeOH, Et_3N	68%	29
$(Ph_4P)_2[Fe_4S_4Cl_4]$	$FeCl_2$ + NaSPh excess + S_8 + $(Ph_4P)Cl$	MeCN	—	20
$(R_4N)_2[Fe_4S_4Cl_4]$	$(R_4N)_2[Fe_4S_4(^tBuS)_4]$ + benzoyl chloride	MeCN	80–92%	26, 27
$(Et_4N)_2[Fe_4S_4Br_4]$	$(Et_4N)_2[Fe_4S_4(^tBuS)_4]$ + benzoyl bromide	MeCN	50–65%	26, 27
$(Et_4N)_2[Fe_4S_4I_4]$	$(Et_4N)_2[Fe_4S_4Cl_4]$ + NaI excess	MeCN	75%	26, 27
$(Pr_4N)_2[Fe_4S_4Cl_4]$	$(Pr_4N)_2[Fe_4S_4(SH)_4]$ + 1,2-dichloroethane	—	85%	28

line $(BTMA)_2[FeI_4]$ was isolated in quantitative yield from those solutions when being exposed to air and moisture.

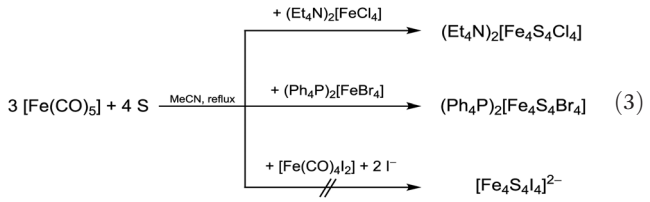

(3)

The iodide cluster $[Fe_4S_4I_4]^{2-}$ was prepared as the $BTMA^+$ salt in high yield (94%) by reproducing Pohl's original procedure using $[Fe(CO)_5]$, sulphur, iodine and iodide (pathway E in Schemes 1 and 3). Synchrotron XRPD (see also later) revealed a small amount of impurities in $(BTMA)_2[Fe_4S_4I_4]$ which could not be identified so far. We tried to recrystallise the product from CH_2Cl_2 at elevated pressure as published.[30,31] Depending on water and oxygen content of the solvent CH_2Cl_2 cluster degradation was observed by UV-vis-NIR spectroscopy and crystals of $(BTMA)_2[FeI_4]$ were found in the resulting material.

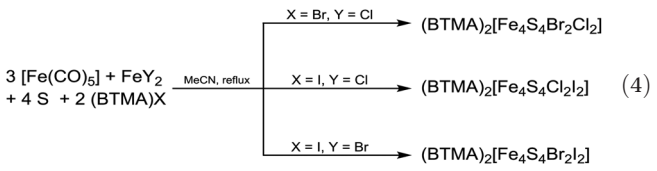

(4)

Reactions using ferrous halides FeY_2 with (BTMA)X under similar conditions lead to formation of the heteroleptic clusters $[Fe_4S_4Br_2Cl_2]^{2-}$, $[Fe_4S_4Cl_2I_2]^{2-}$ and $[Fe_4S_4Br_2I_2]^{2-}$ in MeCN (eqn (4) and Scheme 3). UV-vis-NIR absorption spectroscopy from reaction solutions shows both absorptions bands at 693–702 nm and 1088–1128 nm which are characteristic for $[Fe_4S_4X_4]^{2-}$ clusters (see later in the UV-vis-NIR section).[25] Black crystalline salts of $BTMA^+$ were obtained for all these three cubane clusters in high yields of 77–89% upon ether diffusion. Elemental analysis showed a halide ratio X : Y of 2 : 2 for the bulk materials. This could either mean that the pure $[Fe_4S_4X_2Y_2]^{2-}$ clusters or a mixture of species $[Fe_4S_4X_{4-n}Y_n]^{2-}$ with an averaged X : Y ratio of 2 : 2 are present in these solids. Synchrotron X-ray powder diffraction show that these crystalline materials represent indeed the pure heteroleptic clusters $(BTMA)_2[Fe_4S_4X_2Y_2]$ (see also later).

Remarkably, attempts to prepare heterobimetallic clusters $[MFe_3S_4X_4]^{2-}$ (M = Mn, Co; X = Cl, Br, I) by this method result only in formation of monometallic clusters $[Fe_4S_4X_4]^{2-}$. Various experiments were carried out using $(Et_4N)_2[CoCl_4]$, $(Ph_4P)_2[CoBr_4]$, $CoI_2{\cdot}nH_2O$, $MnI_2{\cdot}4H_2O$ as precursors. The reaction mixtures were analysed by ESI MS and UV-vis-NIR absorption spectroscopy, the materials obtained after precipitation using diethyl ether were characterised by elemental analysis and XRPD. Neither in the reaction mixtures nor in the isolated materials we found evidence for the heterobimetallic clusters. *E.g.* when using $(Et_4N)_2[CoCl_4]$ a MS signal at m/z = 624.1 is found in MeCN solutions which fits well to a $[Et_4N + Fe_4S_4Cl_4]^-$ species concerning peak position and isotopic pattern, whereas no signal at m/z = 626.7 corresponding to a $[Et_4N + CoFe_3S_4Cl_4]^-$ species is observed (Fig. S1, ESI†). Obviously, the transition metal halide only serves as halide source for the assembly of the monometallic cluster. In the case of $(Ph_4P)_2[CoBr_4]$, the precursor could be identified from XRPD analysis in the solid reaction product, the rest of the materials were largely amorphous. For the simple Co or Mn iodides we assume the formation of CoS and MnS which are virtually insoluble in MeCN.

We also attempted to modify Pohl's original method (Scheme 1E) by replacing iodine by bromine or the interhalogens ICl and IBr, respectively. Under similar conditions using

$[Fe(CO)_5]$, sulphur, bromine and bromide $[Fe_4S_4Br_4]^{2-}$ can be prepared in THF solution (eqn (5)).

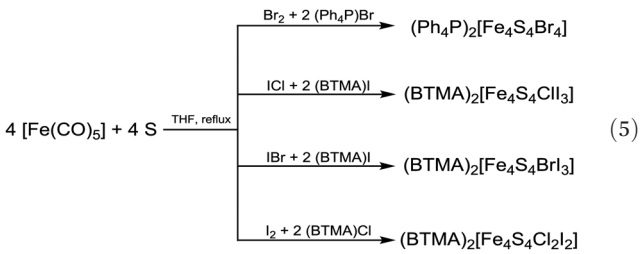

(5)

The tetraphenylphosphonium salt $(Ph_4P)_2[Fe_4S_4Br_4]$ was isolated as a black solid in good yields (Table 1). Its identity and purity was confirmed by XRPD. Analogous reactions using ICl and IBr for the preparation of $[Fe_4S_4X_3Y]^{2-}$ clusters were conducted in THF. Black amorphous solids were isolated upon solvent evaporation that turned out to be mixture of all possible $[Fe_4S_4X_{4-n}Y_n]^{2-}$ clusters. The amorphous character of these solids already indicates that these materials contain very probably a mixture of different clusters. This will be discussed later in detail with ESI MS results. Similar observations can be made from reactions using iodine and chloride in order to form $[Fe_4S_4Cl_2I_2]^{2-}$ clusters (eqn (5)).

Although $[Fe_4S_4X_4]^{2-}$ can be prepared using the previously mentioned halogen/interhalogen pathway it turned out to be ineffective since the procedure is limited to THF as solvent. Unfortunately, solubility of the clusters is quite low in THF. Thus, they precipitate rather quickly and no crystalline material was obtained. Whereas $[Fe_4S_4I_4]^{2-}$ can also be prepared from iodine in MeCN solutions, reactions between bromine or interhalogenes, respectively and the solvent prevent cluster formation.

Negative ESI MS

ESI mass spectra (negative mode) of $(BTMA)_2[Fe_4S_4I_4]$ dissolved in THF is dominated by the molecular peak of the parent ion $[Fe_4S_4I_4]^{2-}$ with m/z = 429.8 (Fig. S2, ESI†). The simulated isotopic pattern fits well to the two-fold negatively charged cluster ion. A further remarkable peak with m/z = 556.6 represents the species $[Fe_2S_2I_3]^-$. This is a product of oxidative cluster degradation. Like thiolate clusters, $[Fe_4S_4X_4]^{2-}$ may decay in the presence of excess ligand with oxidation to binuclear clusters $[Fe_2S_2X_4]^{2-}$ which are converted to $[Fe_2S_2X_3]^-$ losing one ligand.[9,10,25] Furthermore, small quantities of $[FeI_3]^-$ m/z = 437.1 and $[FeI_4]^-$ m/z = 563.2 are present that are formed from $[FeI_4]^{2-}$ by loss of iodide or oxidation, respectively. $[FeI_4]^{2-}$ that was also isolated as BTMA salt from decomposed $[Fe_4S_4I_4]^{2-}$ seems to be a final product of cluster decay.

From diluted solutions of $(BTMA)_2[Fe_4S_4Br_4]$ in acetone a well resolved UHR-ESI (neg. mode) MS was obtained. Fig. 1 represents the molecular peak of $[Fe_4S_4Br_4]^{2-}$, the full MS is provided in the ESI.† The dianion $[Fe_4S_4Br_4]^{2-}$ shows the most intense peak at m/z = 335.6497. Its mass value and its isotopic pattern fit very well to the calculated data (Fig. 1A). The distance between each peak inside the pattern of m/z = 0.5 confirms its dianionic character. A peak at m/z = 821.4260 with slightly lower intensity represents the singly charged [BTMA + $Fe_4S_4Br_4]^-$ species. Extensive fragmentation seems not to be induced at this collision energy. Only weak peaks of $[Fe_4S_4Br_3]^-$ (m/z = 590.3813) and $[Fe_4S_4Br_3O_2]^-$ (m/z = 622.3710) can be detected. They belong to an ion series starting with $[Fe_4S_4Br_4]^{2-}$ which loses one bromide ligand followed by binding an oxygen molecule (Scheme 4). This may be a first step in cluster degradation upon oxidation. Similarly, $[Fe_4S_4Cl_3O_2]^-$ has been detected.[51]

Bromide ions were not detected. Product ions of oxidative splitting of cubane clusters in the presence of excess ligand can only be found in traces. Those are $[Fe_2S_2Br_4]^{2-}$ (m/z = 247.7414) and $[Fe_2S_2Br_3]^-$ (m/z = 414.5670) which belong to an analogous fragmentation series as we have observed for the iodide cluster and what is well-known for thiolate clusters.[9,10,25] Additionally, further adduct species [M + $Fe_4S_4Br_4]^-$ with M = alkali metals can be observed. So, the $[Fe_4S_4Br_4]^{2-}$ cluster turned out to be relatively stable towards decay in the absence of oxygen.

UHR-ESI MS of diluted solutions of the heteroleptic clusters $(BTMA)_2[Fe_4S_4X_2Y_2]$ obtained from the FeY_2/X^- pathway (eqn (4)) in acetone exhibit the presence of all five possible dianionic cluster species represented by the formula $[Fe_4S_4X_{4-n}Y_n]^{2-}$ with the $[Fe_4S_4X_2Y_2]^{2-}$ dianions being the most abundant in case of X = Cl, Y = Br and X = Br, Y = I (Table 2).

Apart of the dianionic $[Fe_4S_4X_{4-n}Y_n]^{2-}$ species also their adducts [BTMA + $Fe_4S_4X_{4-n}Y_n]^-$ are detected (see ESI†). The molecular peaks are well resolved and are in good to very good agreement with calculated isotopic patterns (Fig. 1B–D). For the combination X = Cl, Y = I, the $BTMA^+$ adduct [BMTA + $Fe_4S_4Cl_2I_2]^-$ (m/z = 825.5033) is the most prevalent species, while the dianion $[Fe_4S_4Cl_2I_2]^{2-}$ (m/z = 337.6883) is not the most abundant. The signal for $[Fe_4S_4ClI_3]^{2-}$ (m/z = 383.6560) is also quite intense while the signal for $[Fe_4S_4Cl_3I]^{2-}$ (m/z = 291.7184) almost vanished. Measurements on $(BTMA)_2[Fe_4S_4Cl_2I_2]$ and $(BTMA)_2[Fe_4S_4ClI_3]$ in THF show the same peculiar distribution. For reasons we do not understand so far the $[Fe_4S_4ClI_3]^{2-}$ ion seems to be much more stable than $[Fe_4S_4Cl_2I_2]^{2-}$ under the MS conditions. In contrast to this, the solid sample of $(BTMA)_2[Fe_4S_4Cl_2I_2]$ seems to contain exclusively the $[Fe_4S_4Cl_2I_2]^{2-}$ cluster (see section on synchrotron X-ray powder diffraction).

As found for the $[Fe_4S_4Br_4]^{2-}$ fragmentation series the mixed clusters decompose by loss of one halide ligand and binding of O_2 (Scheme 4). The abundance of these species is quite similar to the distribution of their parent ions $[Fe_4S_4X_{4-n}Y_n]^{2-}$. Product ions of oxidative cluster splitting like $[Fe_2S_2X_{4-n}Y_n]^{2-}$ and $[Fe_2S_2X_{3-n}Y_n]^-$ were not detected (see ESI†).[9,10,25]

The presence of all five possible clusters $[Fe_4S_4X_{4-n}Y_n]^{2-}$ is due to rapid scrambling of X and Y ligands and has been observed for other $[Fe_4S_4]$ clusters in solution.[10,51] This scrambling is usually very fast and is only suppressed if the cluster's total charge is zero (*vide supra*).[9,10,34,36–38,52] When the stock solutions for MS were allowed to stand under inert atmosphere for a day no significant changes to the distributions of $[Fe_4S_4X_{4-n}Y_n]^{2-}$ ions were observed (see ESI†) which means

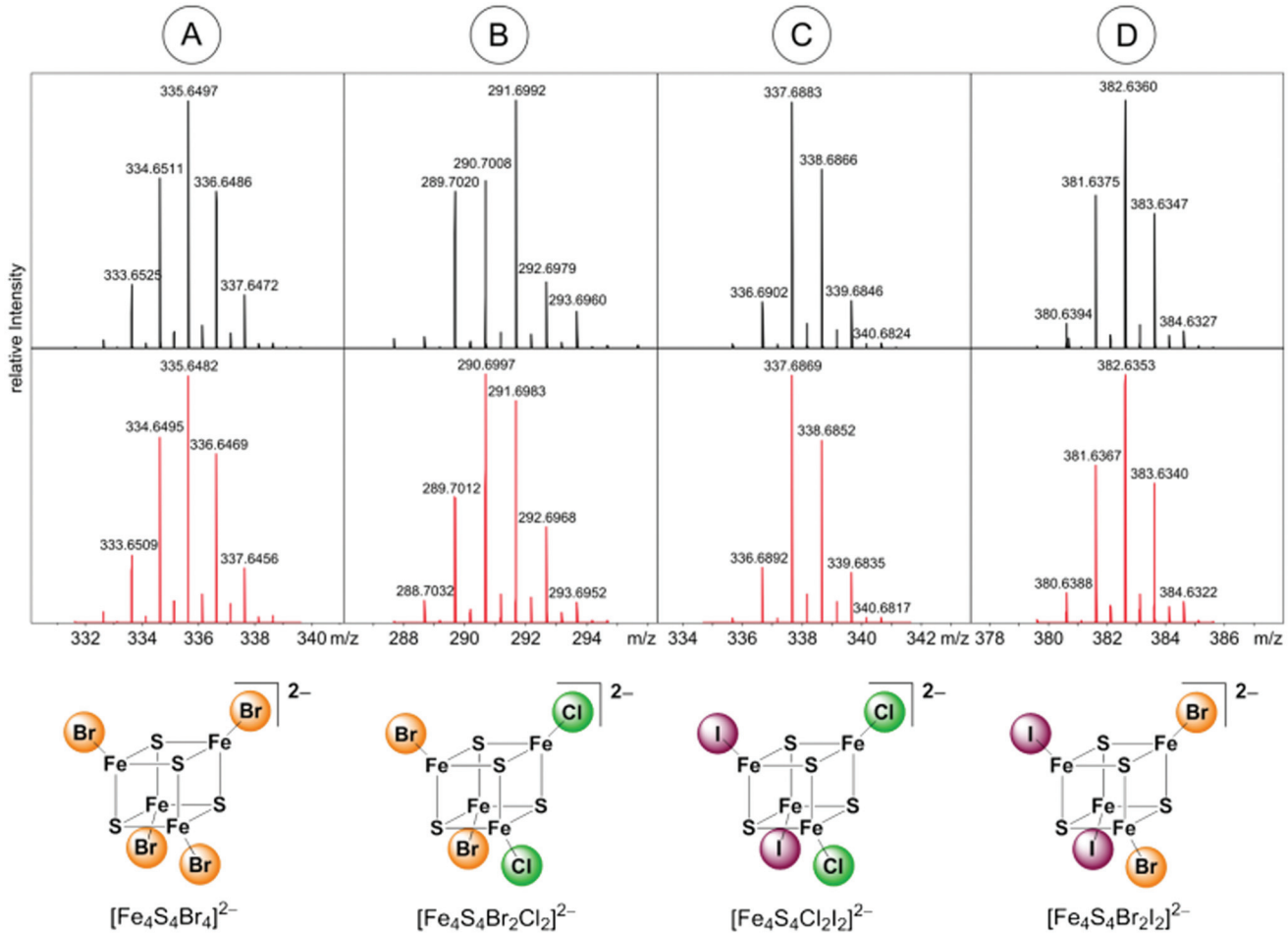

Fig. 1 Molecular peaks of $[Fe_4S_4Br_4]^{2-}$, $[Fe_4S_4Br_2Cl_2]^{2-}$, $[Fe_4S_4\ Cl_2I_2]^{2-}$ and $[Fe_4S_4Br_2I_2]^{2-}$ ions in neg. UHR-ESI MS in acetone (above, collected data; below, simulated isotopic pattern).

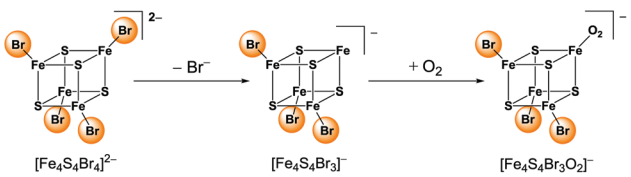

Scheme 4 Ion series of $[Fe_4S_4Br_4]^{2-}$ decay in UHR-ESI source.

that immediately after dissolving the materials equilibria between the different species is obtained.

The ESI MS obtained from THF solutions of $(BTMA)_2[Fe_4S_4Cl_2I_2]$, $(BTMA)_2[Fe_4S_4ClI_3]$ and $(BTMA)_2[Fe_4S_4BrI_3]$ prepared from $[Fe(CO)_5]$ and ICl, IBr or I_2 respectively (eqn (5)) also show distribution of all possible clusters. In contrast to the $(BTMA)_2[Fe_4S_4X_2Y_2]$ materials obtained by the iron(II) halide method (eqn (4)), their spectra exhibit much more different molecular ions containing iron, sulphur and halide. Although we cannot exclude that this difference is due to the solvent (THF *vs.* acetone), we assume that the material already contains cluster mixtures and by-products like prismane clusters which can be identified by their fragments $[Fe_6S_6Cl_2I_3]^{2-}$ and $[Fe_6S_6I_5]^{2-}$ (see ESI†). The rather amorphous character of these materials compared to the crystalline $(BTMA)_2[Fe_4S_4X_2Y_2]$ materials supports this idea.

UV-vis-NIR absorption spectroscopy

UV-vis-NIR absorption spectra have been frequently used to identify $[Fe_4S_4I_4]^{2-}$, $[Fe_4S_4Br_4]^{2-}$, $[Fe_4S_4Cl_4]^{2-}$ and other cluster ions in solution.[22,25,53] Especially, the absorption bands in the visible and near infrared region are good tracers to identify $[Fe_4S_4X_4]^{2-}$ clusters and were utilised by us for reaction control. Samples of $[Fe_4S_4X_4]^{2-}$ and $[Fe_4S_4X_2Y_2]^{2-}$ from preparations with FeX_2 and halide in MeCN show that halide $[Fe_4S_4]$ clusters are present in all reaction mixtures. This is important since from solutions containing $[Fe_4S_4Cl_4]^{2-}$ a solid cubane cluster could not be isolated. Instead, $(BTMA)_3[Fe_6S_6Cl_6]$ was obtained. However, the recorded absorption bands in this case fit well to data reported by Holm and co-workers for $[Fe_4S_4Cl_4]^{2-}$ (Table 3)[25] showing that $[Fe_4S_4Cl_4]^{2-}$ is dominant in the reaction solution. When dissolving the

Table 2 Main molecular cluster ions of $[Fe_4S_4X_{4-n}Y_n]^{2-}$ from negative mode UHR-ESI MS of $(BTMA)_2[Fe_4S_4X_2Y_2]$ in acetone[a]

	m/z (intensity)		
	X = Cl Y = Br	X = Cl Y = I	X = Br Y = I
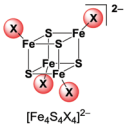 $[Fe_4S_4X_4]^{2-}$	245.7521 (43%)	245.7523 (19%)	335.6488 (15%)
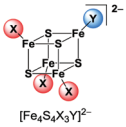 $[Fe_4S_4X_3Y]^{2-}$	268.7258 (19%)	292.7184 (3%)	359.6419 (44%)
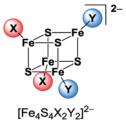 $[Fe_4S_4X_2Y_2]^{2-}$	291.6992 (100%)	337.6883 (46%)	382.6360 (100%)
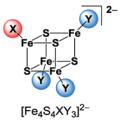 $[Fe_4S_4XY_3]^{2-}$	313.6743 (90%)	383.6560 (100%)	405.6303 (75%)
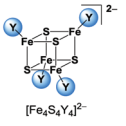 $[Fe_4S_4Y_4]^{2-}$	335.6492 (44%)	429.6239 (42%)	429.6232 (29%)

[a] Characterised by *m/z* values and isotopic pattern. The given intensities were relative intensities in the experiment.

materials $(BTMA)_2[Fe_4S_4Br_4]$ and $(BTMA)_2[Fe_4S_4I_4]$ corresponding spectra were obtained (Fig. 2, Table 3).

The UV-vis-NIR absorption spectra of the heteroleptic clusters $[Fe_4S_4Br_2Cl_2]^{2-}$, $[Fe_4S_4Cl_2I_2]^{2-}$ and $[Fe_4S_4Br_2I_2]^{2-}$ in solution (reaction mixtures and dissolved isolated material) (Fig. 2, Table 3) exhibit very similar absorption bands as the homoleptic clusters $[Fe_4S_4Br_4]^{2-}$ and $[Fe_4S_4I_4]^{2-}$.[25] However, from the MS data we assume that these spectra represent all five possible species from ligand X scrambling (see Table 2). The spectra in the vis-NIR range were dominated by broad absorption bands with maxima around 1100 nm and intense bands around 700 nm (Fig. 2). Further strong absorptions for all compounds were found around 500 nm and the UV range is dominated by very strong absorptions probably due to the $BTMA^+$ cations (Table 3, further spectra in the ESI†).[25]

The absorptions in the visible range have been frequently used to establish the formation or transformation of $[Fe_xS_y]^{n-}$ clusters (x = 2, 3, 4; y = 2 or 4)[54–58] and have been assigned to ligand(X)-to-metal(Fe) charge transfer (LMCT) (at 700 nm), or μ-S/RS-to-metal(Fe) charge transfer (LMCT) (at 500 nm) transitions, respectively.[25,49,54,59,60] In contrast to this, the broad near infrared absorptions with maxima ranging from 1080–1230 nm have been widely ignored. They are present in all $[Fe_4S_4X_4]^{2-}$ clusters (X = halides or thiolates) but their origin remains to be elucidated.[22,25,61] It has been proposed[61] that they are the result of the mixed-valent oxidation state of the $[Fe_4S_4]^{2+}$ core with two ferrous and two ferric centres (Scheme 5).

Multimetallic complexes of osmium,[62] ruthenium[63] and iron[64,65] in mixed-valent oxidation states typically exhibit broad absorption bands in near infrared which were ascribed to so-called intervalence charge transfer (IVCT) or metal-to-metal charge transfer (MMCT).[65–70] These transitions are established for mixed valent compounds as a good measure of the electron delocalisation.[63,71–73] While for $[Fe_2S_2]$ clusters[74,75] and related materials,[76–80] the IVCT character of such low energy absorptions in the NIR range was established by spectroscopy and calculations, for the $[Fe_4S_4]$ clusters this remains to be done, although some mixed valent oligoiron compounds have been studied in this respect.[54,81–83] This goes along with quantum chemical calculations[84,85] finding the binuclear $[Fe_2S_2]$ cluster easier to treat, due to their rather localised character. In contrast to this, higher nuclearity clusters are considered to be partially delocalised, lying between class II and class III according to the Robin and Day classification.[63,71–73,84] Based on this we tentatively assign the near infrared absorption of the $[Fe_4S_4X_4]^{2-}$ and $[Fe_4S_4X_2Y_2]^{2-}$ clusters to IVCT transitions. The electron exchange is mediated by the bridging sulphur ligands in the $[Fe_4S_4]$ core, presumably through the so-called hole transfer mechanism.[62,71–73] Due to the fast electron (or hole) transfer the oxidation state of the iron atoms is averaged to 2.5 (Scheme 5), in line with EPR and Mössbauer experiments on such clusters.[2,7,29,56,61,86] Both the IVCT character of these long-wavelength absorptions and the hole transport mechanism needs to be proven by a quantum mechanical model for the $[Fe_4S_4X_4]^{2-}$ clusters, which is not yet available.

Table 3 UV-vis-NIR absorption maxima λ_{max} of homoleptic $[Fe_4S_4X_4]^{2-}$ and heteroleptic $[Fe_4S_4X_2Y_2]^{2-}$ clusters

	λ_{max} [nm] (ε_λ [cm^{-1} M^{-1}])					
$(BTMA)_2[Fe_4S_4Cl_4]$[a]	260	—	507	690	1078	1202
$(Et_4N)_2[Fe_4S_4Cl_4]$[b]	262	275 sh	505 sh	690	1080	1200
$(BTMA)_2[Fe_4S_4Br_4]$	289 (18 528)	303 sh (17 766)	471 sh (2588)	698 (1900)	1106 (624)	1190 sh (566)
$(BTMA)_2[Fe_4S_4I_4]$	360	390 sh	490 sh	712 sh	1141	1230 sh
$(BTMA)_2[Fe_4S_4Br_2Cl_2]$[c]	278 sh (13 330)	301 sh (11 151)	504 sh (1990)	693 (1591)	1088 (521)	1192 sh (461)
$(BTMA)_2[Fe_4S_4Cl_2I_2]$[c]	315 sh (6376)	353 sh (5711)	492 sh (2259)	698 (1512)	1110 (500)	1174 sh (468)
$(BTMA)_2[Fe_4S_4Br_2I_2]$[c]	276 sh (21 311)	304 sh (19 436)	482 sh (2791)	705 (1700)	1128 (551)	1205 sh (512)

All spectra recorded in MeCN solution. [a] From the reaction mixture. [b] In DMF from ref. 25. [c] The spectra of the compounds containing $[Fe_4S_4X_2Y_2]^{2-}$ represent rather the mixtures of all possible $[Fe_4S_4X_{4-n}Y_n]^{2-}$ species.

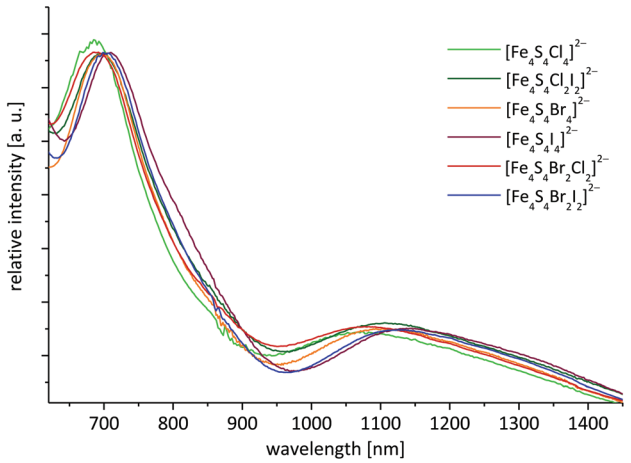

Fig. 2 Long-wavelength part of the UV-vis-NIR absorption spectra of halide cubane clusters in MeCN. The spectra of the $[Fe_4S_4X_2Y_2]^{2-}$ represent rather the mixture of all possible $[Fe_4S_4X_{4-n}Y_n]^{2-}$ species.

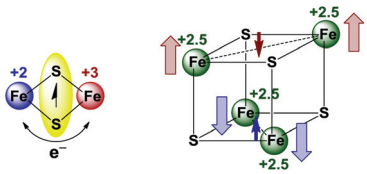

Scheme 5 Electron exchange between ferric and ferrous iron mediated by bridging sulfide ligands (left); magnetic structure of the $[Fe_4S_4]^{2+}$ core (right).[2,7]

For the X-to-Fe LMCT at around 700 nm a slight red-shift with decreasing electronegativity of X (Fig. 2, Table 3) is observed for the homoleptic clusters.[25] For the $[Fe_4S_4X_2Y_2]^{2-}$ clusters this shift is observed as well in a $[Fe_4S_4Br_2Cl_2]^{2-}$ > $[Fe_4S_4Cl_2I_2]^{2-}$ > $[Fe_4S_4Br_2I_2]^{2-}$ sequence, confirming the assignment. From MS experiments we assume that these spectra represent very probably all possible species $[Fe_4S_4X_{4-n}Y_n]^{2-}$ from ligand scrambling, however MS also showed that the species $[Fe_4S_4X_2Y_2]^{2-}$ are dominant in solution. Comparable studies on $[Fe_2S_2X_{4-n}Y_n]^{2-}$ show a similar trend for LMCT absorption bands upon gradual replacement of chloride by bromide.[87]

Also the near infrared IVCT bands show red-shifts with increasing ligand electronegativity. This strongly suggests an influence of the halide ligands to the accepting and donating Fe centred orbitals in these transitions. Like the X-to-Fe LMCT bands the IVCT energies lie also between the associated homoleptic clusters. Unfortunately, the S-to-Fe LMCT absorptions around 500 nm are not well resolved and no correlation of absorption energies and X electronegativity can be made.

Synchrotron X-ray powder diffraction

The structure of $(BTMA)_2[Fe_4S_4I_4]$ (monoclinic, space group *Cc*, $Z = 4$) has been reported by Pohl and co-workers.[31] X-ray powder diffraction (XRPD) should allow to detect whether the new materials were isostructural to this. Phase analysis using synchrotron radiation is preferred over laboratory sources as narrow half-widths and consequent reduction in overlap can be obtained, greatly simplifying the identification of individual reflections.

The XRPD of $(BTMA)_2[Fe_4S_4I_4]$ is in line with simulated data from the published crystal structure (see Fig. S24, ESI†).[31] Closer inspection reveals some additional reflections due to a minor amount of a microcrystalline, so far unknown, by-product. The XRPD data of $(BTMA)_2[Fe_4S_4Br_4]$ shows that this material is indeed isostructural to $(BTMA)_2[Fe_4S_4I_4]$ (Fig. S25, ESI†) and here, no additional reflections of a second phase or impurities are observed.

The XRPDs recorded from $(BTMA)_2[Fe_4S_4Br_2Cl_2]$, $(BTMA)_2$-$[Fe_4S_4Cl_2I_2]$ and $(BTMA)_2[Fe_4S_4Br_2I_2]$ samples are in good agreement with the $(BTMA)_2[Fe_4S_4Br_4]$ pattern (Fig. 3). Slight variations in reflection positions and intensities are due to different lattice parameters and atom types. The reflections do not exhibit a significant broadening (no increased full width at half maximum). It is apparent from this that the sample is homogenous without any phase width. The halide ratio X : Y of 2 : 2 found for these materials by elemental analysis could also represent mixtures of clusters with an average ratio X : Y of 2 : 2. However, XRPD clearly shows that only the defined $[Fe_4S_4X_2Y_2]^{2-}$ clusters are present in the bulk crystalline material.

As can be seen from MS and also UV-vis-NIR spectroscopy, in solutions of $(BTMA)_2[Fe_4S_4X_2Y_2]$ all five possible species $[Fe_4S_4X_{4-n}Y_n]^{2-}$ are present in equilibria with the $[Fe_4S_4X_2Y_2]^{2-}$ clusters being the most abundant. We assume, that upon adding diethyl ether to the reaction mixture (to solutions in THF or MeCN) the most abundant clusters $[Fe_4S_4X_2Y_2]^{2-}$ start to crystallise and the other species $[Fe_4S_4X_{4-n}Y_n]^{2-}$ are consumed through fast exchange equilibria.

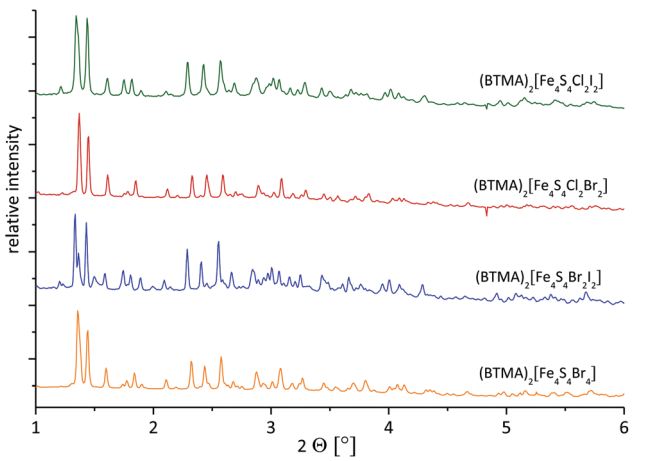

Fig. 3 Synchrotron XRPD of homoleptic $(BTMA)_2[Fe_4S_4Br_4]$ and heteroleptic $(BTMA)_2[Fe_4S_4Br_2Cl_2]$, $(BTMA)_2[Fe_4S_4Cl_2I_2]$ and $(BTMA)_2[Fe_4S_4Br_2I_2]$ clusters (experimental data with λ = 0.207203 Å; recorded at approx. 293 K).

Also for $(BTMA)_2[Fe_4S_4Br_2Cl_2]$, $(BTMA)_2[Fe_4S_4Cl_2I_2]$ and $(BTMA)_2[Fe_4S_4Br_2I_2]$, the monoclinic space group *Cc* can be assumed. As reported for $(BTMA)[Fe_4S_4I_4]^{2-}$,[31] a significant distortion of the $[Fe_4S_4]$ core due to intermolecular halide–halide interactions can be expected in all our clusters with the BTMA cation. This distortion should be stronger in comparison to $[Fe_4S_4]$ clusters in $(Et_4N)_6[(Fe_4S_4I_4)_2(Fe_2S_2I_4)]$ (tetragonal, $P4_2bc$),[30] $(Ph_4P)_2[Fe_4S_4I_4]$ (tetragonal, $I4_1/a$)[31] or in the Ph_4P^+ salts of $[Fe_4S_4Cl_4]^{2-}$, $[Fe_4S_4Br_2Cl_2]^{2-}$ and $[Fe_4S_4Br_4]^{2-}$ (monoclinic, $C2/c$).[29]

The XRPD of $(Ph_4P)_2[Fe_4S_4Br_4]$ (eqn (5)) collected at λ = 0.551155 Å with synchrotron radiation fits well to theoretical data calculated from the published structure with respect to reflection positions (Fig. S26, ESI†).[29] However, the measured intensities show significant deviations from the calculated values, which might be attributed to an inhomogeneous particle shape (preferred orientation). Furthermore, the experimental data exhibit a high background, which might be due to amorphous phases. This is in line with the generally more pronounced amorphous character of the materials produced by this method (eqn (5)) (see MS section).

Vibrational spectroscopy

Solid samples (as polyethylene pellets) of $(BTMA)_2[Fe_4S_4Br_4]$ exhibit four dominant vibrations bands in far IR. From comparison with $[Fe_4S_4X_4]^{2-}$ salts (X = Cl, Br, I) of Ph_4P^+ and Bu_4N^+ the 377 cm^{-1} frequency can be assigned to stretching ν_{as}(Fe–S) modes of the $[Fe_4S_4]$ core and is invariant for all examined clusters in the form of $BTMA^+$ salts (Fig. 4 and Table 4).[29,88–91] A significant blue-shift to higher energies is observed for the corresponding Ph_4P^+ and Bu_4N^+ salts. This can be ascribed to specific interactions in the crystal structures of $(cation)_2[Fe_4S_4X_4]$ compounds.

Table 4 FIR frequencies for $[Fe_4S_4X_4]^{2-}$ and $[Fe_4S_4X_2Y_2]^{2-}$ [a]

	ν_{as} (Fe–S) core	ν_{as} (Fe–X) terminal	ν(Fe–S) core (I)	ν(Fe–S) core (II)
$(Ph_4P)_2[Fe_4S_4Cl_4]$ [b]	382 (w)	353 (s)	—	—
$(Bu_4N)_2[Fe_4S_4Cl_4]$ [c]	389	360	278	253
$(BTMA)_2[Fe_4S_4Br_4]$	377 (m)	307 (s)	269 (w) 260 (sh)	227 (w)
$(Ph_4P)_2[Fe_4S_4Br_4]$ [b]	382 (w)	305 (s)	—	—
$(Bu_4N)_2[Fe_4S_4Br_4]$ [c]	384	310	279	230/242
$(BTMA)_2[Fe_4S_4I_4]$	377 (s)	289 (s)	273 (s) 258 (m)	229 (m)
$(Bu_4N)_2[Fe_4S_4I_4]$ [c]	381	296	264	232
$(Ph_4P)_2[Fe_4S_4Br_2Cl_2]$ [b]	380 (m)	354 (s) 305 (s)	—	—
$(BTMA)_2[Fe_4S_4Cl_2I_2]$	378 (m)	356 (s) 290 (s)	272 (m) 260 (m)	229 (w)
$(BTMA)_2[Fe_4S_4Br_2Cl_2]$	378 (m)	356 (s) 306 (s)	270 (m) 260 (sh)	232 (w)
$(BTMA)_2[Fe_4S_4Br_2I_2]$	376 (m)	306 (s) 291 (s)	272 (sh) 260 (m)	231 (w)

[a] From measurement of microcrystalline samples as polyethylene pellets, in [cm^{-1}]. [b] From ref. 29. [c] From ref. 88.

In the structure of $(BTMA)_2[Fe_4S_4I_4]$ (monoclinic, *Cc*) an attractive intermolecular interaction to two individual iodide ligands of each cluster lead to a one-dimensional network of $[Fe_4S_4X_4]^{2-}$ cluster across the structure.[31] Thus, the symmetry of the $[Fe_4S_4]$ core is significantly reduced in the $BTMA^+$ salts compared to the corresponding structures of Ph_4P^+ and Bu_4N^+ salts.[31] It is reasonable to assume that lower cluster symmetry goes along with lower vibration energies of typical cluster core vibrations. This is roughly the case when comparing typical vibrations in Table 4.

The stretching ν(Fe–Br) modes of the terminal bromido ligands were recorded for $(BTMA)_2[Fe_4S_4Br_4]$ at 307 cm^{-1} following the trend of published data.[29,88] In addition, bands at 269, 260 and 227 cm^{-1} can be assigned to vibrational modes of bridging Fe–S bonds similar to those reported for the Bu_4N^+ salt.[89–91] Like the ν_{as}(Fe–S) vibrations they are blue-shifted but also split due to symmetry reduction in the $BTMA^+$ structure.

The frequencies found for the ν(Fe–S) stretching modes in heteroleptic clusters $[Fe_4S_4Br_2Cl_2]^{2-}$, $[Fe_4S_4Cl_2I_2]^{2-}$ and $[Fe_4S_4Br_2I_2]^{2-}$ are consistent with those of the homoleptic bromide and iodine clusters. For the ν(Fe–X) modes it seems that in each case two individual bands were observed for the heteroleptic clusters with about 355 cm^{-1} for Fe–Cl, 306 cm^{-1} for Fe–Br and 290 cm^{-1} for Fe–I groups. Those frequencies do not differ from those found in homoleptic clusters.

This is remarkable since the idealised symmetry of the 2 : 2 coordinated clusters is already reduced from T_d to C_{2v} (Scheme 6) which should have an effect on the vibrational modes. The shifts and splitting of the bands that might be expected upon symmetry reduction seem to be merged within the broad bands. Thus only the broadening of the bands indi-

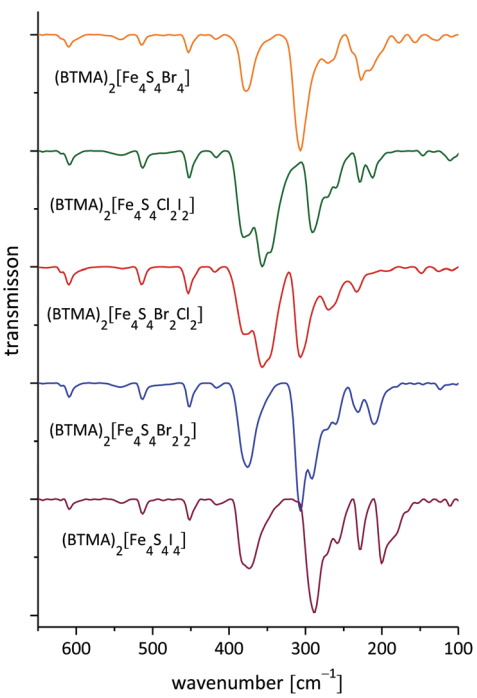

Fig. 4 FIR spectra of BTMA halide $[Fe_4S_4]$ cluster salts.

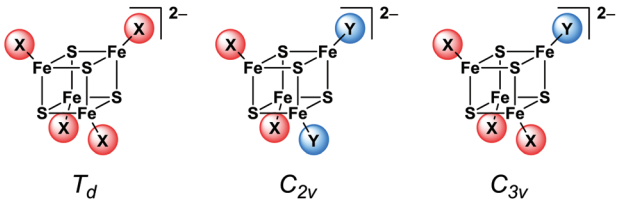

Scheme 6 Idealised cluster symmetry.

cates the loss of symmetry in the structures. On the other hand, orientation effects in the crystal structure probably overrule the molecular symmetry of the clusters.

Conclusions

By evaluating the scope of a previously reported method to prepare $[Fe_4S_4I_4]^{2-}$ from $[Fe(CO)_5]$, sulphur and iodide sources a couple of new improved preparations for $[Fe_4S_4X_4]^{2-}$ clusters with various combinations of chloride, bromide and iodide were developed. The utilisation of simple iron(II) halide precursors like iron(II) halide and tetrahalidoferrates(II) has turned out to be the most efficient way to produce these clusters in high yields and purities (see Table 1). But even more valuable is its convenience as an one-pot, nearly atom-economic procedure which offers broad applicability of these clusters towards utilisation as precursors for the preparation of functionalised $[Fe_4S_4]$ containing materials. Further variations of the reaction conditions and efforts to extend this method also to the synthesis of heterobimetallic clusters $[MFe_3S_4X_4]^{2-}$ (M = Mn, Co; X = Cl, Br, I) have been less successful but have provided some insight into the mechanisms of formation of such clusters.

Besides the reproduction of the established homoleptic $[Fe_4S_4Cl_4]^{2-}$, $[Fe_4S_4Br_4]^{2-}$ and heteroleptic $[Fe_4S_4Br_2Cl_2]^{2-}$ clusters, the new clusters $[Fe_4S_4Cl_2I_2]^{2-}$ and $[Fe_4S_4Br_2I_2]^{2-}$ were isolated and characterised for the first time. The application of synchrotron XRPD revealed the isostructural analogy between the clusters in solid state as salts of $BTMA^+$ (= benzyltrimethylammonium). Thus, a similar high distortion of the cluster ions in these structures like in the previously reported $(BTMA)_2[Fe_4S_4I_4]$ (monoclinic, space group *Cc*) can be assumed. This is confirmed by NIR vibrational spectroscopy through significant differences of typical $[Fe_4S_4]$ core vibrations when comparing the $BTMA^+$ salts with Ph_4P^+ or Bu_4N^+ derivatives.

In the solid the $(BTMA)_2[Fe_4S_4X_2Y_2]$ materials are homogenous and consist only of $[Fe_4S_4X_2Y_2]^{2-}$ clusters, which is evident from XRPD. When dissolved a rapid halide ligand exchange produces mixtures of $[Fe_4S_4X_{4-n}Y_n]^{2-}$ clusters as revealed by negative UHR-ESI MS. All these species are also observed in the reaction mixtures. However, upon crystallisation, the main component of such a mixture, the desired $[Fe_4S_4X_2Y_2]^{2-}$ cluster, seems to crystallise selectively giving the pure materials $(BTMA)_2[Fe_4S_4X_2Y_2]$. In contrast to this, during the crystallisation of solutions containing mainly $[Fe_4S_4Cl_4]^{2-}$ (MS and UV-vis-NIR) $(BTMA)_3[Fe_6S_6Cl_6]$ is obtained, containing the hexanuclear prismane-shaped cluster $[Fe_6S_6Cl_6]^{3-}$. We assume that although the tetranuclear species is dominating the reaction mixture, further cluster species (hexanuclear, binuclear, ...) are present, interconnected through rearrangement reactions. Proper choice of the cations is in both cases a good option to obtain pure compounds out of the mixtures of cluster species we observed in all of the investigated preparation methods. Another is surely the use of polydentate ligands.

UV-vis-NIR spectroscopy reveals characteristic near infrared absorptions for homoleptic $[Fe_4S_4X_4]^{2-}$ and heteroleptic clusters $[Fe_4S_4X_2Y_2]^{2-}$ and for the latter very probably a mixture of $[Fe_4S_4X_{4-n}Y_n]^{2-}$ species is observed. Due to the variation of X and Y the bands around 700 nm can clearly be assigned to X-to-Fe LMCT transitions The long-wavelength absorptions around 1100 nm are also slightly influenced by the variation of X and Y and were assigned to IVCT transitions within the mixed valent $[Fe_4S_4]^{2+}$ core. The details of the electronic structure of the heteroleptic clusters are of certain interest and will be focus of our future efforts.

Experimental section

Materials and procedures

All manipulations and sample preparations were performed under anaerobic and dry argon atmosphere (>99 996%, Airproducts) using standard Schlenk and high-vacuum techniques or a MBraun labmaster 130 dry box. Glassware was flame-dried immediately before use. THF was dried using a MBRAUN MB SPS-800 solvent purification system and degassed by pump-freeze–thaw techniques. Diethyl ether was distilled under argon from sodium/benzophenone and MeCN from calcium hydride prior to use. Commercially available $[Fe(CO)_5]$ was filtered through a pad of sea sand and silica and stored under argon atmosphere. Further chemicals were used as purchased. $(Et_4N)_2[FeCl_4]$ and $(Ph_4P)_2[FeBr_4]$ have been prepared similar to published procedures.[50]

Instrumentation

Elemental analysis was obtained using a Hekatech CHNS EuroEA 3000 analyzer. To complete combustion samples have been analysed with additional V_2O_5 in an atmosphere with 20 ml of oxygen. UV-vis-NIR absorption spectra were recorded in solution on a PerkinElmer Lambda 950 UV/Vis Scan spectrophotometer. IR spectra were collected with a Bruker IFS66νS spectrometer. Samples have been prepared as polyethylene pellet (abbreviations s = strong, m = medium, w = weak, sh = shoulder). ESI mass spectra with THF and MeCN solutions have been recorded with an APPLIED BIOSYSTEMS LC/MS system API 5000 at a collision energy of 10 eV and a potential of 5000 V. Sample solutions in THF were diluted to concentrations of 10^{-5} to 10^{-6} M and introduced to the machine with a 1–5 μL flow rate. Tubes and the machine have been purged

with pure argon immediately before each use. For data analysis APPLIED BIOSYSTEMS software ANALYST 1.4.2 was utilised. UHR-ESI MS measurements of acetone solutions were performed on a UHR-TOF Bruker Daltonik (Bremen, Germany) maXis 5G, an ESI-TOF MS capable of resolution of at least 60 000 FWHM. Detection was in negative-ion mode and the source voltage was 3.2 kV. The flow rates were 250 μL per hour. The machine was calibrated prior to every experiment *via* direct infusion of the Agilent ESI-TOF low concentration tuning mixture, which provided an *m*/*z* range of singly charged peaks up to 2700 Da in both ion modes. Preliminary X-ray powder diffraction data collection under laboratory conditions was carried out with a Huber G670 diffractometer using Guinier geometry and germanium-monochromatised Mo-K(α)1 radiation. For reflection detection *image-plate* techniques were used. Synchrotron data collection was performed at DESY (Hamburg, beamline P02.1, storage ring Petra III with λ = 0.207203 Å and a PerkinElmer XRD 1621 flat panel detector) or at DELTA (Dortmund, beamline 9 with λ = 0.551155 Å, silicon (311) double crystal monochromator and a MARRESEARCH MAR 345 flat panel detector). Samples have been measured in capillaries sealed in an argon atmosphere (0.5 mm diameter). The collected data was transformed with Fit2d[92] and analysed with WinXPow.[93]

Cluster preparations with halogens and interhalogens

$(BTMA)_2[Fe_4S_4I_4]$ (Method A in THF, see Scheme 1) 1.27 g (5.0 mmol) iodine, 0.64 g (20.0 mmol) sulphur and 2.77 g (10.0 mmol) (BTMA)I were suspended in 100 ml THF. To the stirred slurry 2.70 ml (20.5 mmol) $[Fe(CO)_5]$ was added in small portions. Upon heating the mixture under reflux for 19 h its colour changed to black. After cooling the solvent was evaporated to dryness under reduced pressure and the remaining black microcrystalline solid was dried in vacuum at 50 °C for 20 min. **Yield:** 5.46 g (94%). **(−)ESI-MS** (THF): *m*/*z* (%) = 429.8 (95) $[Fe_4S_4I_4]^{2-}$, 556.6 (28) $[Fe_2S_2I_3]^-$. **Elemental analysis** for $C_{20}H_{32}I_4Fe_4N_2S_4$ (1159.74): calcd C 20.71, H 2.78, N 2.42, S 11.06; found C 20.65, H 2.77, N 2.25, S 11.22. **FIR** (PE pellet): ν_{max} [cm^{-1}]: 610 (w), 513 (w), 452 (m), 416 (w), 377 (s), 289 (s), 273 (sh), 258 (m), 227 (m), 198 (m), 183 (sh). **UV-vis-NIR:** λ_{max} (MeCN) [nm]: 292, 319 (sh), 361, 392 (sh), 493 (sh), 708.

(Method B in MeCN) 1.27 g (5.0 mmol) iodine, 0.64 g (20.0 mmol) sulphur and 2.77 g (10.0 mmol) (BTMA)I were suspended in 40 ml MeCN. To the stirred slurry 2.70 ml (20.5 mmol) $[Fe(CO)_5]$ was added. The mixture was heated under reflux for 16 h and a colour change to black could be observed. After cooling the reaction mixture was filtered through a frit. The filtrate was layered with 200 ml diethyl ether and stored for 3 days at −18 °C. Black needles precipitated from the solution were filtered off and dried in vacuum. **Yield:** 4.66 g (81%). **Elemental analysis** for $C_{20}H_{32}I_4Fe_4N_2S_4$ (1159.74): calcd C 20.71, H 2.78, N 2.42, S 11.06; found C 20.71, H 2.63, N 2.55, S 10.89. **UV-vis-NIR:** λ_{max} (MeCN) [nm]: 247, 291, 320 (sh), 360, 390 (sh), 490 (sh), 709, 1141, 1230 (sh).

$(Ph_4P)_2[Fe_4S_4Br_4]$ 4.19 g (10.0 mmol) $(Ph_4P)Br$ and 0.65 g (20.0 mmol) sulphur were suspended in 100 ml THF and cooled to 0 °C. After addition of 0.50 ml (9.8 mmol) bromine 2.70 ml (20.0 mmol) $[Fe(CO)_5]$ was added drop wise within 2 min. The reaction mixture was stirred for 5 min and then heated under reflux for 39 h. Upon heating a black solid precipitated from the dark red solution. The black microcrystalline solid was collected by filtration, washed with 3 × 10 ml THF and dried in vacuum for 10 min. By layering the combined filtrates with 260 ml diethyl ether a second crop of black microcrystals could be obtained. **Yield over all fractions:** 4.78 g (71%).

$(BTMA)_2[Fe_4S_4BrI_3]$ 2.77 g (10.0 mmol) (BTMA)I, 0.64 g (20.0 mmol) sulphur and 1.03 g (5.0 mmol) iodine monobromide were suspended in 100 ml THF and cooled to −30 °C. 2.7 ml (20.0 mmol) $[Fe(CO)_5]$ was added in portions of 0.5 ml within 2 min causing a strong evolution of gas. Gradually, the reaction mixture turned black. After removing the cooling bath the mixture was allowed to warm up and was finally heated under reflux for 21 h. The solvent was removed under reduced pressure at 40 °C. A sticky black mass was obtained by drying the remaining residue for 1 h in vacuum at 50 °C. **Yield:** 4.51 g (81%). **(−)ESI-MS** (THF): *m*/*z* (%) = 429.7 (95) $[Fe_4S_4I_4]^{2-}$, 405.8 (58) $[Fe_4S_4BrI_3]^{2-}$, 382.8 (23) $[Fe_4S_4Br_2I_2]^{2-}$, 358.8 (8) $[Fe_4S_4Br_3I]^{2-}$, 335.8 (10) $[Fe_4S_4Br_4]^{2-}$.

$(BTMA)_2[Fe_4S_4ClI_3]$ A slurry of 2.77 g (10.0 mmol) (BTMA)I and 0.64 g (20.0 mmol) sulphur in 100 ml THF was cooled to −60 °C. After addition of 0.25 ml (5.0 mmol) iodine monochloride 2.7 ml (20.0 mmol) $[Fe(CO)_5]$ was added in small portions to the orange coloured suspension. While warming up to room temperature a strong evolution of gas could be observed from the mixture. Upon heating under reflux for 23 h the mixture's colour changed slowly to black. The solvent was removed under reduced pressure at 35 °C. A sticky black mass was obtained by drying the remaining residue for 2 h in vacuum at 50 °C. **Yield:** 5.00 g (94%). **(−)ESI-MS** (THF): *m*/*z* (%) = 580.4 (60) $[Fe_6S_6I_5]^{2-}$, 548.6 (64) $[Fe_6S_4I_5]^{2-}$, 429.7 (87) $[Fe_4S_4I_4]^{2-}$, 383.7 (35) $[Fe_4S_4ClI_3]^{2-}$, 337.8 (29) $[Fe_4S_4Cl_2I_2]^{2-}$, 291.9 (5) $[Fe_4S_4Cl_3I]^{2-}$, 246.1 (18) $[Fe_4S_4Cl_4]^{2-}$.

$(BTMA)_2[Fe_4S_4Cl_2I_2]$ To a slurry of 1.86 g (10.0 mmol) (BTMA)Cl, 0.64 g (10.0 mmol) sulphur and 1.27 g (5.0 mmol) iodine in 150 ml THF 2.7 ml (20.0 mmol) $[Fe(CO)_5]$ was added in small portions of 0.5 ml within 2 min. An intensive evolution of gas could be observed from the reddish-brown suspension turning slowly to black upon heating under reflux for 89 h. After cooling the solvent was evaporated to dryness under reduced pressure. The remaining residue was dried for 4 h at 70 °C in vacuum yielding a black sticky mass. **Yield:** 3.78 g (75%). **(−)ESI-MS** (THF): *m*/*z* (%) = 580.4 (94) $[Fe_6S_6I_5]^{2-}$, 548.6 (100) $[Fe_6S_4I_5]^{2-}$, 488.7 (40) $[Fe_6S_6Cl_2I_3]^{2-}$, 456.5 (50) $[Fe_6S_4Cl_2I_3]^{2-}$, 429.7 (30) $[Fe_4S_4I_4]^{2-}$, 383.7 (20) $[Fe_4S_4ClI_3]^{2-}$, 337.8 (18) $[Fe_4S_4Cl_2I_2]^{2-}$, 291.9 (3) $[Fe_4S_4Cl_3I]^{2-}$, 246.1 (47) $[Fe_4S_4Cl_4]^{2-}$.

Cluster preparations with ferrous tetrahalidoferrates $[FeX_4]^{2-}$

$(Et_4N)_2[Fe_4S_4Cl_4]$ To a slurry of 1.74 g (3.8 mmol) $(Et_4N)_2[FeCl_4]$ and 0.49 g (15.2 mmol) sulphur in 120 ml MeCN 1.50 ml (11.4 mmol) $[Fe(CO)_5]$ were added *via* syringe. The yellow reac-

tion mixture was heated under reflux for 17 h. A colour change to black could be observed upon heating. The solvent was evaporated to dryness under reduced pressure. The remaining residue was dried in vacuum at 50 °C for 15 min yielding a black microcrystalline powder. **Yield:** 1.99 g (69%). **(−)ESI-MS** (MeCN): *m*/*z* (%) = 624.0 (26) $[Et_4N + Fe_4S_4Cl_4]^-$, 492.9 (55) $[Fe_4S_4Cl_4]^-$, 365.5 (45) $[Fe_3S_4Cl_2]^-$, 282.9 (60) $[Fe_2S_2Cl_3]^-$, 245.6 (100) $[Fe_4S_4Cl_4]^{2-}$.

$(Ph_4P)_2[Fe_4S_4Br_4]$ To a slurry of 1.00 g (1.0 mmol) $(Ph_4P)_2[FeBr_4]$ and 0.12 g (3.8 mmol) sulphur in 30 ml MeCN 0.38 ml (2.9 mmol) $[Fe(CO)_5]$ were added. The reaction mixture was heated under reflux for 1 day. Upon heating the reaction mixture turned black quickly. The solvent was evaporated to dryness under reduced pressure. The remaining residue was dried in vacuum at 50 °C for 1 h yielding a black microcrystalline powder. **Yield:** 1.18 g (92%).

Cluster preparations with ferrous halides

$(BTMA)_2[Fe_4S_4Cl_4]$ respectively $(BTMA)_3[Fe_6S_6Cl_6]$ 1.28 g (10.1 mmol) $FeCl_2$, 1.28 g (40.0 mmol) sulphur and 3.71 g (20.0 mmol) (BTMA)Cl were suspended in 40 ml MeCN. After addition of 3.94 ml (30.0 mmol) $[Fe(CO)_5]$ the resulting orange mixture was heated under reflux for 3 days. A colour change to black was observed immediately upon heating. The mixture was allowed to cool and filtered through a frit. UV-vis reaction control confirms $[Fe_4S_4Cl_4]^{2-}$ in solution. **UV-vis-NIR:** λ_{max} (MeCN) [nm]: 260, 507, 690, 1078, 1202 (sh).

The black filtrate was layered with 160 ml of diethyl ether and stored for 3 weeks at −18 °C. Black column-shaped crystals were filtered off and dried under vacuum. **Yield:** 7.18 g (91%). **Elemental analysis** for $C_{30}H_{48}Cl_6Fe_6N_3S_6$ (1190.35): calcd C 30.26, H 4.06, N 3.53, S 16.16; found C 30.38, H 4.07, N 3.71, S 16.09. **FIR** (PE pellet): ν_{max} [cm^{-1}]: 612 (w), 513 (w), 454 (m), 419 (w), 381 (sh), 351 (s), 300 (m), 283 (sh), 250 (sh), 200 (w), 214 (w).

$(BTMA)_2[Fe_4S_4Br_4]$ 1.11 g (5.1 mmol) $FeBr_2$, 0.64 g (20.0 mmol) sulphur and 2.30 g (10.0 mmol) (BTMA)Br were suspended in 40 ml MeCN. After addition of 1.97 ml (15.0 mmol) $[Fe(CO)_5]$ the resulting orange mixture was heated under reflux for 1 day. The suspension turned black quickly upon heating. The mixture was allowed to cool down and filtered through a frit. The black filtrate was layered with 180 ml of diethyl ether and stored for 3 weeks at −18 °C. Black needle-shaped crystals were filtered off and dried under vacuum. **Yield:** 4.20 g (87%). **(−)ESI-MS** (acetone): *m*/*z* (%) = 335.6479 (100) $[Fe_4S_4Br_4]^{2-}$, 821.4260 (60) $[BTMA + Fe_4S_4Br_4]^-$, 590.3813 (4) $[Fe_4S_4Br_3]^-$, 622.3710 (4) $[Fe_4S_4Br_3O_2]^-$, 671.2970 (4) $[Fe_4S_4Br_4]^-$, 694.2866 (2) $[Na + Fe_4S_4Br_4]^-$, 678.3131 (7) $[Li + Fe_4S_4Br_4]^-$. **Elemental analysis** for $C_{20}H_{32}Br_4Fe_4N_2S_4$ (971.37): calcd C 24.72, H 3.32, N 2.88, S 13.20; found C 24.53, H 3.46, N 2.99, S 13.25. **FIR** (PE pellet): ν_{max} [cm^{-1}]: 610 (w), 515 (w), 453 (m), 418 (w), 377 (s), 307 (s), 269 (w), 260 (sh), 227 (m), 214 (w). **UV-vis:** λ_{max} (MeCN) [nm]: 240, 261 (sh), 269, 289, 303 (sh), 469 (sh), 507 (sh), 697, 1106, 1190 (sh).

$(BTMA)_2[Fe_4S_4Cl_2I_2]$ 1.27 g (10.0 mmol) $FeCl_2$, 1.28 g (40.0 mmol) sulphur and 5.54 g (20.0 mmol) (BTMA)I were suspended in 40 ml MeCN. After addition of 4.00 ml (30.3 mmol) $[Fe(CO)_5]$ the resulting orange mixture was heated under reflux for 6 h and then stirred overnight. A colour change to black was observed immediately upon heating. The mixture was allowed to cool and filtered through a frit. The black filtrate was layered with 150 ml of diethyl ether and stored for 3 days at −18 °C. Black needle-shaped crystals were filtered off and dried under vacuum. A second crystalline crop was obtained from the filtrate upon storing it for additional 16 weeks at −18 °C. **Yield over all fractions:** 7.48 g (77%). **(−) ESI-MS** (acetone): *m*/*z* (%) = 429.6239 (42) $[Fe_4S_4I_4]^{2-}$, 383.6560 (100) $[Fe_4S_4ClI_3]^{2-}$, 337.6883 (46) $[Fe_4S_4Cl_2I_2]^{2-}$, 292.7184 (3) $[Fe_4S_4Cl_3I]^{2-}$, 245.7523 (19) $[Fe_4S_4Cl_4]^{2-}$, 1009.3728 (2) $[BTMA + Fe_4S_4I_4]^-$, 917.4389 (9) $[BTMA + Fe_4S_4ClI_3]^-$, 825.5033 (15) $[BTMA + Fe_4S_4Cl_2I_2]^-$, 733.5675 (9) $[BTMA + Fe_4S_4Cl_3I]^-$, 643.6284 (3) $[BTMA + Fe_4S_4Cl_4]^-$, 732.3404 (<1) $[Fe_4S_4I_3]^-$, 640.4057 (7) $[Fe_4S_4ClI_2]^-$, 548.4708 (21) $[Fe_4S_4Cl_2I]^-$, 456.5353 (16) $[Fe_4S_4Cl_3]^-$, 764.3302 (<1) $[Fe_4S_4I_3O_2]^-$, 672.3954 (5) $[Fe_4S_4ClI_2O_2]^-$, 580.4606 (17) $[Fe_4S_4Cl_2IO_2]^-$, 488.5251 (12) $[Fe_4S_4Cl_3O_2]^-$. **Elemental analysis** for $C_{20}H_{32}Cl_2I_2Fe_4N_2S_4$ (976.47): calcd C 24.59, H 3.30, N 2.87, S 13.13; found C 24.45, H 3.25, N 2.77, S 12.95. **FIR** (PE pellet): ν_{max} [cm^{-1}]: 609 (w), 513 (w), 452 (m), 416 (w), 378 (s), 356 (s), 346 (sh), 290 (s), 272 (m), 260 (m), 228 (m), 212 (m). **UV-vis-NIR:** λ_{max} (MeCN) [nm]: 315 (sh), 353 (sh), 492 (sh), 695, 1110, 1174 (sh).

$(BTMA)_2[Fe_4S_4Br_2Cl_2]$ 1.27 g (10.0 mmol) $FeCl_2$, 1.28 g (40.0 mmol) sulphur and 4.60 g (20.0 mmol) (BTMA)Br were suspended in 40 ml MeCN. After addition of 4.00 ml (30.3 mmol) iron $[Fe(CO)_5]$ the resulting orange mixture was heated under reflux for 17 h. A colour change to black was observed immediately upon heating. The mixture was left to stand for 3 days and was then filtered through a frit. The black filtrate was layered with 200 ml of diethyl ether and stored for 3 days at −18 °C. Black needle-shaped crystals were filtered off and dried under vacuum. **Yield:** 7.81 g (89%). **(−)ESI-MS** (acetone): *m*/*z* (%) = 335.6492 (44) $[Fe_4S_4Br_4]^{2-}$, 313.6743 (90) $[Fe_4S_4Br_3Cl]^{2-}$, 291.6992 (100) $[Fe_4S_4Br_2Cl_2]^{2-}$, 268.7258 (19) $[Fe_4S_4BrCl_3]^{2-}$, 245.7521 (43) $[Fe_4S_4Cl_4]^{2-}$, 821.4248 (11) $[BTMA + Fe_4S_4Br_4]^-$, 777.4755 (36) $[BTMA + Fe_4S_4Br_3Cl]^-$, 731.5284 (47) $[BTMA + Fe_4S_4Br_2Cl_2]^-$, 687.5786 (27) $[BTMA + Fe_4S_4BrCl_3]^-$, 643.6280 (6) $[BTMA + Fe_4S_4Cl_4]^-$, 590.3805 (2) $[Fe_4S_4Br_3]^-$, 546.4314 (13) $[Fe_4S_4Br_2Cl]^-$, 502.4818 (24) $[Fe_4S_4BrCl_2]^-$, 456.5348 (11) $[Fe_4S_4Cl_3]^-$, 622.3699 (1) $[Fe_4S_4Br_3O_2]^-$, 578.4210 (10) $[Fe_4S_4Br_2ClO_2]^-$, 534.4714 (17) $[Fe_4S_4BrCl_2O_2]^-$, 488.5246 (8) $[Fe_4S_4Cl_3O_2]^-$. **Elemental analysis** for $C_{20}H_{32}Cl_2Br_2Fe_4N_2S_4$ (882.47): calcd C 27.21, H 3.17, N 3.65, S 14.53; found C 27.23, H 3.08, N 3.66, S 14.69. **FIR** (PE pellet): ν_{max} [cm^{-1}]: 609 (w), 515 (w), 453 (m), 419 (w), 378 (m), 356 (s), 347 (sh), 306 (s), 270 (m), 260 (sh), 233 (m). **UV-vis-NIR:** λ_{max} (MeCN) [nm]: 261, 278 (sh), 301 (sh), 504 (sh), 689, 1088, 1192 (sh).

$(BTMA)_2[Fe_4S_4Br_2I_2]$ 2.16 g (10.0 mmol) $FeBr_2$, 1.28 g (40.0 mmol) sulphur and 5.54 g (20.0 mmol) (BTMA)I were suspended in 40 ml MeCN. After addition of 4.00 ml (30.3 mmol) $[Fe(CO)_5]$ the resulting orange mixture was heated to reflux for 16 h. The suspension turned black quickly upon heating. The mixture was allowed to cool and filtered through

a frit. The black filtrate was layered with 195 ml of diethyl ether and stored for 3 days at −18 °C. Black needle-shaped crystals were filtered off and dried under vacuum. **Yield:** 9.03 g (85%). **(−)ESI-MS** (acetone): *m*/*z* (%) = 429.6232 (28) $[Fe_4S_4I_4]^{2-}$, 405.6303 (72) $[Fe_4S_4BrI_3]^{2-}$, 382.6360 (96) $[Fe_4S_4Br_2I_2]^{2-}$, 359.6419 (42) $[Fe_4S_4Br_3I]^{2-}$, 335.6488 (14) $[Fe_4S_4Br_4]^{2-}$, 1009.3717 (2) [BTMA + $Fe_4S_4I_4]^-$, 961.3868 (7) [BTMA + $Fe_4S_4BrI_3]^-$, 915.3993 (14) [BTMA + $Fe_4S_4Br_2I_2]^-$, 867.4132 (9) [BTMA + $Fe_4S_4Br_3I]^-$, 821.4241 (2) [BTMA + $Fe_4S_4Br_4]^-$, 732.3395 (<1) $[Fe_4S_4I_3]^-$, 684.3543 (2) $[Fe_4S_4BrI_2]^-$, 638.3662 (5) $[Fe_4S_4Br_2I]^-$, 590.3805 (6) $[Fe_4S_4Br_3]^-$, 764.3295 (<1) $[Fe_4S_4I_3O_2]^-$, 716.3439 (1) $[Fe_4S_4BrI_2O_2]^-$, 670.3558 (4) $[Fe_4S_4Br_2IO_2]^-$, 622.3701 (4) $[Fe_4S_4Br_3O_2]^-$. **Elemental analysis** for $C_{20}H_{32}Br_2I_2Fe_4N_2S_4$ (1065.37): calcd C 22.54, H 3.03, N 2.63, S 12.03; found C 22.48, H 2.99, N 2.51, S 12.16. **FIR** (PE pellet): ν_{max} [cm^{-1}]: 609 (w), 514 (w), 452 (m), 416 (w), 376 (s), 306 (s), 291 (s), 272 (m), 260 (m), 232 (m), 210 (m). **UV-vis-NIR:** λ_{max} (MeCN) [nm]: 276 (sh), 304 (sh), 482 (sh), 702, 1128, 1205 (sh).

Acknowledgements

The authors are grateful to Dr Stefan Liebig, Ireneus Grzesiak and Dr Stefanie Busch, Institute for Inorganic Chemistry, Cologne, Germany, for fruitful discussions and help on X-ray powder diffraction. We are indebted to HASYLAB at DESY, Hamburg, Germany and DELTA, Dortmund, Germany for the kind support of synchrotron radiation. Dr Dennis Rokitta, Hospital of the University of Cologne, Department of Pharmacology, Clinical Pharmacology Unit, is thanked for providing the opportunity for ESI mass spectrometry measurements. The work was financially supported for AOS by DAAD and CONICET; for AK by DFG KL1194/13-1. AF, AOS and FD are members of CONICET. I.I.-B. and M.D. gratefully acknowledge support through the "Solar Technologies Go Hybrid" initiative of the State of Bavaria.

Notes and references

1 M. C. Kennedy, T. A. Kent, M. Emptage, H. Merkle, H. Beinert and E. Münck, *J. Biol. Chem.*, 1984, **259**, 14463–14471.
2 H. Beinert, R. H. Holm and E. Münck, *Science*, 1997, **277**, 653–659.
3 D. C. Johnson, D. R. Dean, A. D. Smith and M. K. Johnson, *Annu. Rev. Biochem.*, 2005, **74**, 247–281.
4 M. K. Johnson and A. D. Smith, Iron-Sulfur Proteins, in *Encyclopedia of Inorganic and Bioinorganic Chemistry*, John Wiley & Sons, Ltd, 2011, pp. 2589–2619.
5 C. Greco, M. Bruschi, P. Fantucci, U. Ryde and L. De Gioia, *J. Am. Chem. Soc.*, 2011, **133**, 18742–18749.
6 I. Span, K. Wang, W. Wang, J. Jauch, W. Eisenreich, A. Bacher, E. Oldfield and M. Groll, *Angew. Chem., Int. Ed.*, 2013, **125**, 2172–2175.
7 H. Beinert, *J. Biol. Inorg. Chem.*, 2000, **5**, 2–15.
8 R. H. Holm, *Acc. Chem. Res.*, 1977, **10**, 427–434.
9 R. H. Holm, in *Comprehensive Coordination Chemistry II*, Pergamon, Oxford, 2003, ch. 8.3, pp. 61–90.
10 P. Venkateswara Rao and R. H. Holm, *Chem. Rev.*, 2004, **104**, 527–559.
11 S. C. Lee, W. Lo and R. H. Holm, *Chem. Rev.*, 2014, **114**, 3579–3600.
12 K. Tanifuji, N. Yamada, T. Tajima, T. Sasamori, N. Tokitoh, T. Matsuo, K. Tamao, Y. Ohki and K. Tatsumi, *Inorg. Chem.*, 2014, **53**, 4000–4009.
13 A. Alwaaly, I. Dance and R. A. Henderson, *Chem. Commun.*, 2014, **50**, 4799–4802.
14 I. Dance and R. A. Henderson, *Dalton Trans.*, 2014, **43**, 16213–16226.
15 I. Dance, *Dalton Trans.*, 2015, **44**, 4707–4717.
16 C. T. Saouma, W. D. Morris, J. W. Darcy and J. M. Mayer, *Chem. – Eur. J.*, 2015, **21**, 9256–9260.
17 C. J. Pickett, S. K. Ibrahim and D. L. Hughes, *Faraday Discuss.*, 2000, **116**, 235–244.
18 P. V. Vanitha and P. O'Brien, *J. Am. Chem. Soc.*, 2008, **130**, 17256–17257.
19 M. Akhtar, J. Akhter, M. A. Malik, P. O'Brien, F. Tuna, J. Raftery and M. Helliwell, *J. Mater. Chem.*, 2011, **21**, 9737.
20 B. D. Yuhas, A. L. Smeigh, A. P. Samuel, Y. Shim, S. Bag, A. P. Douvalis, M. R. Wasielewski and M. G. Kanatzidis, *J. Am. Chem. Soc.*, 2011, **133**, 7252–7255.
21 V. C.-C. Wang, M. Can, E. Pierce, S. W. Ragsdale and F. A. Armstrong, *J. Am. Chem. Soc.*, 2013, **135**, 2198–2206.
22 Y. Shim, B. D. Yuhas, S. M. Dyar, A. L. Smeigh, A. P. Douvalis, M. R. Wasielewski and M. G. Kanatzidis, *J. Am. Chem. Soc.*, 2013, **135**, 2330–2337.
23 Y. Shim, R. M. Young, A. P. Douvalis, S. M. Dyar, B. D. Yuhas, T. Bakas, M. R. Wasielewski and M. G. Kanatzidis, *J. Am. Chem. Soc.*, 2014, **136**, 13371–13380.
24 M. Schwarz and C. Röhr, *Inorg. Chem.*, 2015, **54**, 1038–1048.
25 G. B. Wong, M. A. Bobrik and R. H. Holm, *Inorg. Chem.*, 1978, **17**, 578–584.
26 B. M. Segal, H. R. Hoveyda and R. H. Holm, *Inorg. Chem.*, 1998, **37**, 3440–3443.
27 M. A. Bobrik, K. O. Hodgson and R. H. Holm, *Inorg. Chem.*, 1977, **16**, 1851–1858.
28 K. Bates, M. Wouldhave and R. A. Henderson, *Dalton Trans.*, 2008, 6527–6529.
29 A. Müller, N. H. Schladerbeck, E. Krickemeyer, H. Bögge, K. Schmitz, E. Bill and A. X. Trautwein, *Z. Anorg. Allg. Chem.*, 1989, **570**, 7–36.
30 W. Saak and S. Pohl, *Z. Naturforsch., B: Anorg. Chem. Org. Chem.*, 1985, **40**, 1105–1112.
31 S. Pohl and W. Saak, *Z. Naturforsch., B: Chem. Sci.*, 1988, **43**, 457–462.
32 M. G. Kanatzidis, N. C. Baenziger, D. Coucouvanis, A. Simopoulos and A. Kostikas, *J. Am. Chem. Soc.*, 1984, **106**, 4500–4511.

33 D. Coucouvanis, M. G. Kanatzidis, E. Simhon and N. C. Baenziger, *J. Am. Chem. Soc.*, 1982, **104**, 1874–1882.
34 W. Saak and S. Pohl, *Z. Naturforsch., B: Chem. Sci.*, 1988, **43**, 813–817.
35 M. A. Tyson, K. D. Demadis and D. Coucouvanis, *Inorg. Chem.*, 1995, **34**, 4519–4520.
36 U. Bierbach, W. Saak, D. Haase and S. Pohl, *Z. Naturforsch., B: Chem. Sci.*, 1991, **46**, 1629–1634.
37 S. Pohl and U. Bierbach, *Z. Naturforsch., B: Chem. Sci.*, 1991, **46**, 68–74.
38 F. Osterloh, W. Saak and S. Pohl, *J. Am. Chem. Soc.*, 1997, **119**, 5648–5656.
39 R. H. Holm, *Pure Appl. Chem.*, 1998, **70**, 931–938.
40 T. Terada, K. Hirabayashi, D. Liu, T. Nakamura, T. Wakimoto, T. Matsumoto and K. Tatsumi, *Inorg. Chem.*, 2013, **52**, 11997–12004.
41 D. L. Gerlach, D. Coucouvanis and N. Lehnert, *Eur. J. Inorg. Chem.*, 2013, 3883–3890.
42 E. P. L. van der Geer, Q. Li, G. v. Koten, R. J. M. Klein Gebbink and B. Hessen, *Inorg. Chim. Acta*, 2008, **361**, 1811–1818.
43 C. Walsdorff, W. Saak and S. Pohl, *J. Chem. Soc., Dalton Trans.*, 1997, 1857–1861.
44 C. Walsdorff, W. Saak, D. Haase and S. Pohl, *Chem. Commun.*, 1997, 1931–1932.
45 J. Zhou, Z. Hu, E. Münck and R. H. Holm, *J. Am. Chem. Soc.*, 1996, **118**, 1966–1980.
46 T. D. P. Stack, J. A. Weigel and R. H. Holm, *Inorg. Chem.*, 1990, **29**, 3745–3760.
47 T. D. P. Stack and R. H. Holm, *J. Am. Chem. Soc.*, 1987, **109**, 2546–2547.
48 E. Victor and S. J. Lippard, *Inorg. Chem.*, 2014, **53**, 5311–5320.
49 M. G. Kanatzidis, W. R. Hagen, W. R. Dunham, R. K. Lester and D. Coucouvanis, *J. Am. Chem. Soc.*, 1985, **107**, 953–961.
50 N. S. Gill, F. B. Taylor, W. E. Hatfield, W. E. Parker, C. S. Fountain and F. L. Bunger, *Inorg. Synth.*, 2007, **9**, 136–142.
51 Y.-J. Fu, J. Laskin and L.-S. Wang, *Int. J. Mass Spectrom.*, 2006, **255–256**, 102–110.
52 M. Harmjanz, C. Junghans, U.-A. Optiz, B. Bahlmann and S. Pohl, *Z. Naturforsch., B: Chem. Sci.*, 1996, **51**, 1040–1048.
53 S. Rutchik, S. Kim and M. A. Walters, *Inorg. Chem.*, 1988, **27**, 1513–1515.
54 J.-F. You, B. S. Snyder, G. C. Papaefthymiou and R. H. Holm, *J. Am. Chem. Soc.*, 1990, **112**, 1067–1076.
55 H. Gao, S. Subramanian, J. Couturier, S. G. Naik, S.-K. Kim, T. Leustek, D. B. Knaff, H.-C. Wu, F. Vignols, B. H. Huynh, N. Rouhier and M. K. Johnson, *Biochemistry*, 2013, **52**, 6633–6645.
56 B. Zhang, S. Bandyopadhyay, P. Shakamuri, S. G. Naik, B. H. Huynh, J. Couturier, N. Rouhier and M. K. Johnson, *J. Am. Chem. Soc.*, 2013, **135**, 15153–15164.
57 M. M.-J. Couture, V. J. J. Martin, W. W. Mohn and L. D. Eltis, *Biochim. Biophys. Acta*, 2006, **1764**, 1462–1469.
58 A. D. Smith, G. N. L. Jameson, P. C. Dos Santos, J. N. Agar, S. Naik, C. Krebs, J. Frazzon, D. R. Dean, B. H. Huynh and M. K. Johnson, *Biochemistry*, 2005, **44**, 12955–12969.
59 Y.-J. Kim and J.-H. Han, *Bull. Korean Chem. Soc.*, 2012, **33**, 48–54.
60 B. V. DePamphilis, B. A. Averill, T. Herskovitz, L. Que Jr. and R. H. Holm, *J. Am. Chem. Soc.*, 1974, **96**, 4159–4167.
61 L. M. Lawson Daku, J. Pécaut, A. Lenormand-Foucaut, B. Vieux-Melchior, P. Iveson and J. Jordanov, *Inorg. Chem.*, 2003, **42**, 6824–6850.
62 W. Kaim and G. K. Lahiri, *Angew. Chem., Int. Ed.*, 2007, **46**, 1778–1796.
63 W. Kaim and B. Sarkar, *Coord. Chem. Rev.*, 2007, **251**, 584–594.
64 M. I. Belinsky, *J. Magn. Magn. Mater.*, 2007, **310**, e486–e488.
65 M. I. Belinsky, *Chem. Phys.*, 1999, **240**, 303–311.
66 W. Kaim, *Coord. Chem. Rev.*, 2011, **255**, 2503–2513.
67 C. Díaz and A. Arancibia, *Polyhedron*, 2000, **19**, 2679–2687.
68 W.-Q. Chen, Y.-M. Chen, T. Lei, W. Liu and Y. Li, *Inorg. Chem. Commun.*, 2012, **19**, 4–9.
69 W. Kaim and B. Schwederski, *Coord. Chem. Rev.*, 2010, **254**, 1580–1588.
70 W. Kaim, *Eur. J. Inorg. Chem.*, 2012, 343–348.
71 W. Kaim, A. Klein and M. Glöckle, *Acc. Chem. Res.*, 2000, **33**, 755–763.
72 D. M. D'Alessandro and F. R. Keene, *Chem. Rev.*, 2006, **106**, 2270–2298.
73 D. M. D'Alessandro and F. R. Keene, *Chem. Soc. Rev.*, 2006, **35**, 424–440.
74 A. Albers, S. Demeshko, S. Dechert, E. Bill, E. Bothe and F. Meyer, *Angew. Chem., Int. Ed.*, 2011, **50**, 9191–9194.
75 J. M. McCormick and E. I. Solomon, *J. Am. Chem. Soc.*, 1990, **112**, 2005–2007.
76 F. Li, M. Chakrabarti, Y. Dong, K. Kauffmann, E. L. Bominaar, E. Münck and L. Que Jr., *Inorg. Chem.*, 2012, **51**, 2917–2929.
77 M. Glöckle, N. E. Katz, M. Ketterle and W. Kaim, *Inorg. Chim. Acta*, 2002, **336**, 55–60.
78 M. Glöckle, W. Kaim, A. Klein, E. Roduner, G. Hübner, S. Zalis, J. van Slageren, F. Renz and P. Gütlich, *Inorg. Chem.*, 2001, **40**, 2256–2262.
79 U. Pfaff, A. Hildebrandt, D. Schaarschmidt, T. Hahn, S. Liebing, J. Kortus and H. Lang, *Organometallics*, 2012, **31**, 6761–6771.
80 R. Warratz, H. Aboulfadl, T. Bally and F. Tuczek, *Chem. – Eur. J.*, 2009, **15**, 1604–1617.
81 K. L. Taft, G. C. Papaefthymiou and S. J. Lippard, *Inorg. Chem.*, 1994, **33**, 1510–1520.
82 K. L. Taft, A. Caneschi, L. E. Pence, C. D. Delfs, G. C. Papaefthymiou and S. J. Lippard, *J. Am. Chem. Soc.*, 1993, **115**, 11753–11766.
83 P. Albores and E. Rentschler, *Inorg. Chem.*, 2010, **49**, 8953–8961.

84 E. I. Solomon, X. Xie and A. Dey, *Chem. Soc. Rev.*, 2008, **37**, 623–638.
85 M. Parthey and M. Kaupp, *Chem. Soc. Rev.*, 2014, **43**, 5067–5088.
86 E. Bill, *Hyperfine Interact.*, 2011, **205**, 139–147.
87 C. Tonon, H. Iernoa, J. Jordanov, J. Laugier and J.-M. Greneche, *Chem. Ber.*, 1997, **130**, 235–239.
88 A. Kern, C. Näther and F. Tuczek, *Inorg. Chem.*, 2004, **43**, 5011–5020.
89 K. Nakamoto, in *Infrared and Raman Spectra of Inorganic and Coordination Compounds: Applications in Coordination, Organometallic, and Bioinorganic Chemistry*, John Wiley & Sons, 5th edn, 1997, vol. B.
90 Y. Xiao, M. Koutmos, D. A. Case, D. Coucouvanis, H. Wang and S. P. Cramer, *J. Chem. Soc., Dalton Trans.*, 2006, 2192–2201.
91 D. Mitra, S. J. George, Y. Guo, S. Kamali, S. Keable, J. W. Peters, V. Pelmenschikov, D. A. Case and S. P. Cramer, *J. Am. Chem. Soc.*, 2013, **135**, 2530–2543.
92 A. P. Hammersley, *FIT2D, V10.3*, ESRF, Grenoble, France, 1998.
93 *STOE WinXPow, version 3.01.03*, STOE and Cie GmbH, Darmstadt, Germany, 2010.